CERN-INTC-2004-016
INTC-P-186
26 April 2004

A Proposal to
the ISOLDE and Neutron Time-of-Flight Experiments
Committee

Studies of a Target System for a 4-MW, 24-GeV Proton Beam

J. Roger J. Bennett[1], Luca Bruno[2], Chris J. Densham[1], Paul V. Drumm[1], T. Robert Edgecock[1], Adrian Fabich[2], Tony A. Gabriel[3], John R. Haines[3], Helmut Haseroth[2], Yoshinari Hayato[4], Steven J. Kahn[5], Jacques Lettry[2], Changguo Lu[6], Hans Ludewig[5], Harold G. Kirk[5], Kirk T. McDonald[6], Robert B. Palmer[5], Yarema Prykarpatskyy[5], Nicholas Simos[5], Roman V. Samulyak[5], Peter H. Thieberger[5], Koji Yoshimura[4]

Spokespersons: H.G. Kirk, K.T. McDonald
Local Contact: H. Haseroth

Abstract

We propose to perform a proof-of-principle test of a target station suitable for a Neutrino Factory or Muon Collider source using a 24-GeV proton beam incident on a target consisting of a free mercury jet that is inside a 15-T capture solenoid magnet. This test could be performed in the TT2A tunnel of the nTOF proton line (upstream of the spallation target). The tests would require only ≈ 100 fast-extracted pulses of full PS intensity, delivered in a pulse-on-demand mode of operation over about 2 weeks. The main piece of apparatus is the LN_2-precooled, 15-T copper magnet of total volume slightly over 1 m^3 with a 15-cm-diameter warm bore. The principle diagnostic is a high-speed optical camera. The mercury jet is part of a closed mercury loop that includes an insert into the bore of the magnet.

[1]CCLRC Rutherford Appleton Laboratory, Chilton, Didcot Oxon, UK OX11 0QX
[2]CERN, CH-1211 Genève 23, Switzerland
[3]Oak Ridge National Laboratory, Oak Ridge, TN 37831, USA
[4]KEK, 1-1 Oho, Tsukuba, Ibaraki 305-0801 Japan
[5]Brookhaven National Laboratory, Upton, NY 11973 USA
[6]Joseph Henry Laboratories, Princeton University, Princeton, NJ 08544 USA

Executive Summary

We propose to perform a proof-of-principle demonstration of a target system based on a free mercury jet, including magnetic focusing/capture of secondary pions/muons, suitable for use in a 4-MW, 24-GeV proton beam as part of a neutrino "superbeam" and/or neutrino factory facility.

The proposed studies emphasize the survival of a prototype target system against issues of single proton pulses: dispersal of the jet target by mechanical "shock" and/or vaporization due to energy deposition by the proton beam, and possible damping of these effects by the strong magnetic field of the capture solenoid. A first phase of such studies has been carried out at BNL and CERN, in which the interaction of a mercury jet with a proton beam, and with a 20-T solenoid magnet, have been investigated separately, with encouraging results. Long-term issues of radiation damage and materials fatigue are to be addressed in separate studies.

- The studies proposed here are to be made using small numbers ($< 1{,}000$ total) of intense 24-GeV proton pulses in the CERN Neutron Time-of-Flight beamline. Of these pulses, only about 40 will be used for studies of the interaction of the proton beam with the mercury jet; the other pulses are for beam tuning.
- A "pulse-on-demand" mode of operation is desired, in which a proton pulse is used at most every few minutes. A higher repetition rate would be useful during beam setup.
- The studies should be carried out in an area suitable for use with a primary proton beam, such at the TT2A tunnel. The small number of beam pulses required will, however, limit the activation of materials to low levels.
- The target system + surrounding 15-T solenoid magnet could occupy as little as 2 m along the beamline. If the solenoid magnet axis is tilted horizontally with respect to the proton beam axis as desired, then the solenoid should be immediately followed by a vertical trim magnet with field integral of 1 T-m.
- The beam should be focusable to a spot of rms radius ≈ 2 mm at the target location.
- The main mode of beam delivery from the CERN PS should be single-turn extraction of up to 4 rf bunches, for a total of 2×10^{13} protons. However, it is desirable to be able to extract any number from 1 to 8 of these bunches during a single turn. A programmable fast-kicker is required for this.
- The mercury jet is to be about 1-cm diameter, flowing at 10-20 m/sec, entirely within a stainless-steel containment vessel (with beam entrance and exit windows of a high-strength alloy). Diagnostics of the beam/jet interaction are primarily optical.
- The pulsed magnet is advantageously operated at about 70K to lower the resistance of its copper coils. A LN_2 storage dewar of at least 6,000 liters is required.
- The magnet requires a special power supply, capable of 4.6 MW peak power.

Contents

1 The Challenge of High-Power Targetry

Intense proton sources pose significant challenges for targets placed in the proton beam, particularly for future upgrades to beam powers of several MWatt. The physics opportunities associated with such intense proton sources are so rich that the challenges must be met. These opportunities include:

- Studies of neutrino oscillations with long baseline neutrino beams both from pion decay [1, 2] and from muon decay [3, 4, 5].
- Studies of rare processes initiated by muons [6, 7, 8].
- Studies of materials with neutrons beams from a spallation source [9, 10, 11].
- Accelerator production of tritium [12].
- Accelerator transmutation of waste [13].
- Accelerator test facilities for fusion reactor materials [14].

The technical challenges for targets in high-power proton beams are threefold:

- Survival of components against melting/vaporization.
- Survival of components against beam-induced pressure waves, in the case of pulsed proton beams.
- Survival of components against radiation damage.

Passive solid targets (or rotating-wheel targets), typically water cooled, have been used in most applications with less than 1-MW beam power. But for beam power in excess of 1 MW such passive solid targets become very problematic in view of the challenges listed above. This has led to consideration of flowing liquid targets: mercury, molten lead, molten Pb/Bi, *etc.*

Liquid target systems still require solid-walled containment vessels and beam windows that isolate the target region from the rest of the accelerator complex. Experience has shown that if a liquid target is confined inside a metal pipe in the region of the interaction with a pulsed proton beam, then the beam-induced pressure waves can cause pitting (associated with cavitation during the negative-pressure phases of the waves) and possible failure of the solid wall [15, 16, 17].

Such concerns indicate that it would be preferable to have a flowing liquid target in the form of a free jet, at least in the region of interaction with the proton beam.

A benchtop demonstration of a free mercury jet was made in 1988 by Johnson [18], as shown in Fig. 1. However, this prototype jet target was never exposed to a proton beam.

During a conceptual study for a $\mu \rightarrow e$ conversion experiment [19], it was realized that surrounding the target by a high-field solenoid magnet (a kind of magnetic bottle) is very effective in maximizing the yield of low-energy secondary pions and muons. This scenario is also very relevant for a muon collider [20] and for a neutrino factory based on a muon storage ring [5, 21].

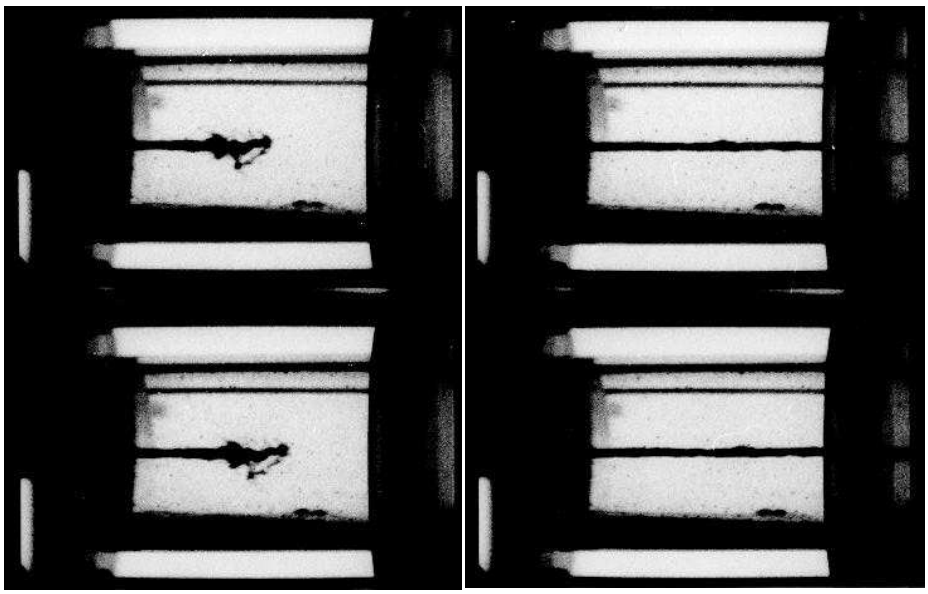

Figure 1: Photographs of a 3-mm-diameter mercury jet.

The present proposal is for a full-scale test of this target concept, in which a mercury jet flows through a 15-T (pulsed) solenoid magnet while interacting with intense, 24-GeV proton pulses extracted from the CERN PS.

1.1 The Target Concept

Sketches of the target concept [21] are shown in Fig. 2.

A continuous mercury jet crosses a proton beam at an angle of about 40 mrad so that the interaction region is approximately two interaction lengths.

The axes of both the proton beam and mercury jet are tilted with respect to the axis of the solenoid magnet by about 100 mrad, which improves the yield of soft pions at large angles, and permits the noninteracting part of the proton beam to be absorbed in the collection pool of mercury.

The magnetic field is large ($\approx$ 20 T) at the interaction region, but falls off to $\approx$ 1 T over several meters, which field strength is then maintained in the subsequent pion decay channel.

The magnetic field profile over the interaction region is improved by use of an iron plug at the upstream end of the magnet, through which the proton beam and flowing mercury must pass.

If the solenoid field is over 14 T, a hybrid construction must be used, with a 14-T superconducting outer coil plus a, say, 6-T inner copper coil that serves also as a radiation shield for the superconducting coil.

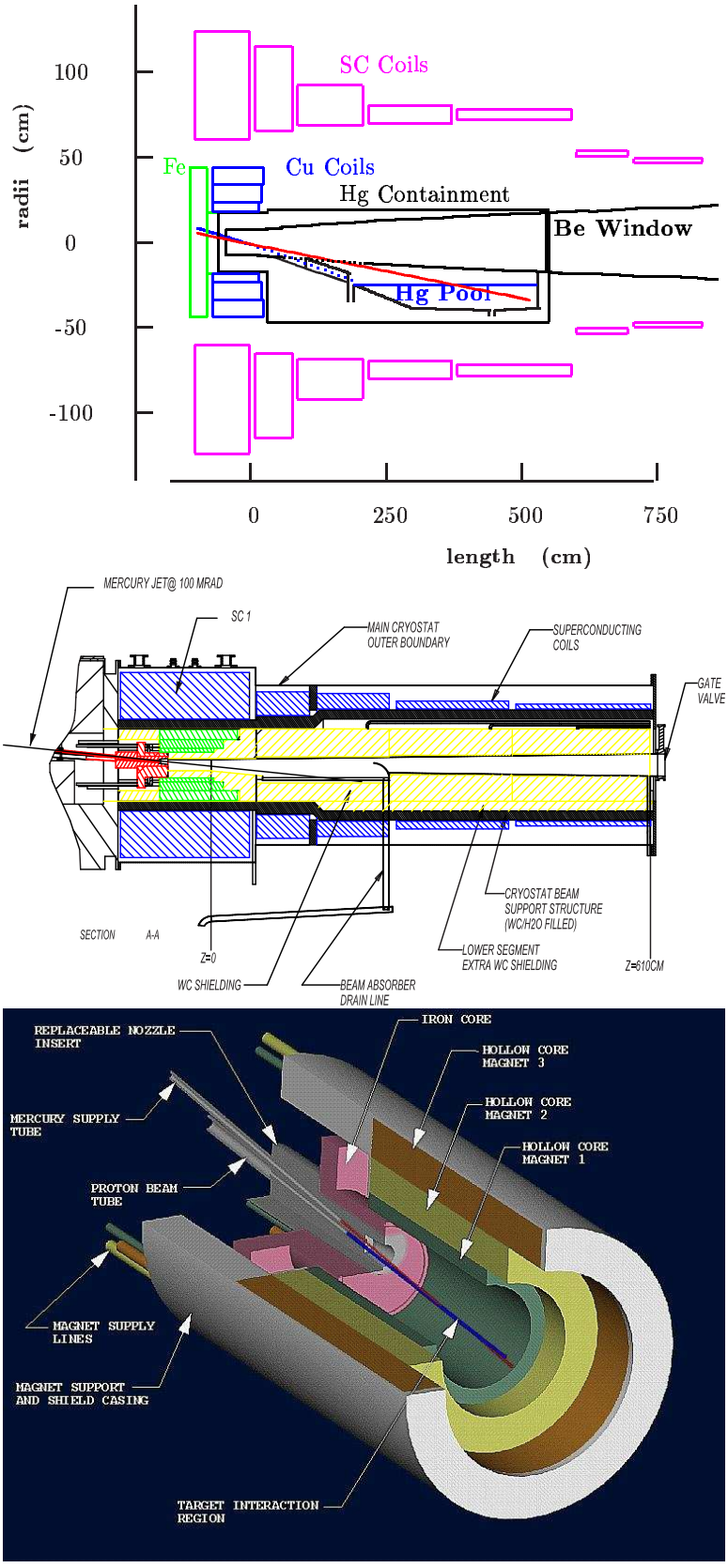

Figure 2: Sketches of the concept of a 4-MW target system in which the proton beam and a mercury jet interact at an angle to the axis of a 20-T solenoid magnet.

The entire assembly of inner coil, iron plug, mercury collection pool and downstream beam window is to be replaceable via remote-handling equipment, as the lifetime of these components is estimated to be only about 15 MW-years.

Representative simulations [22] in support of this target concept, based on the MARS Monte Carlo code [23], are shown in Fig. 3.

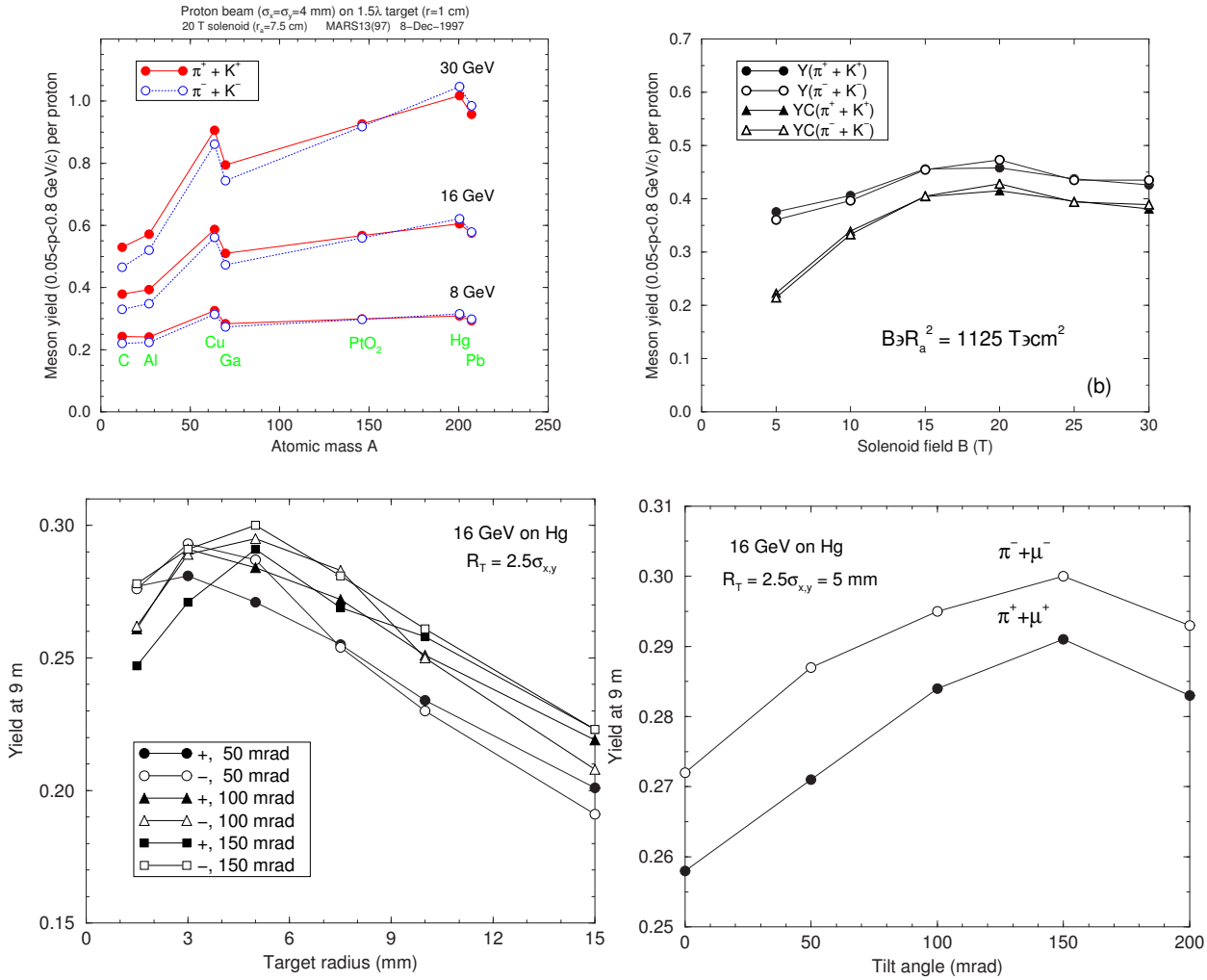

Figure 3: a) Meson yield $(\pi + K)$ from a 1.5-λ_I, 1-cm-radius target irradiated with 8, 16 and 30-GeV proton beams as a function of target atomic mass; b) Meson yield from a 3-λ_I, 1-cm-radius gallium target tilted at angle 150 mrad in a 16-GeV proton beam *vs.* solenoid field strength for a fixed adiabatic invariant BR_a^2; c) Meson yield as a function of target radius; d) Meson yield *vs.* tilt angle between the axis of the capture solenoid and the proton beam.

The simulations indicate that the useful yield of soft pions and muons is improved by

a) The use of a high-Z target material, if the proton beam energy is more than 8 GeV.

b) The use of a capture solenoid field of 15-20 T.

c) The use of a relatively narrow target, 5 mm radius, with RMS proton beam radius of 2 mm.

d) Tilting the beam and jet axis with respect to the magnetic axis by 100-150 mrad.

Simulations have also been made of radiation dose in target system components, to assess lifetime issues. Figure 4 shows a representative result from the MARS calculation [24], and Table 1 indicates the inferred lifetimes against radiation damage of a few key components.

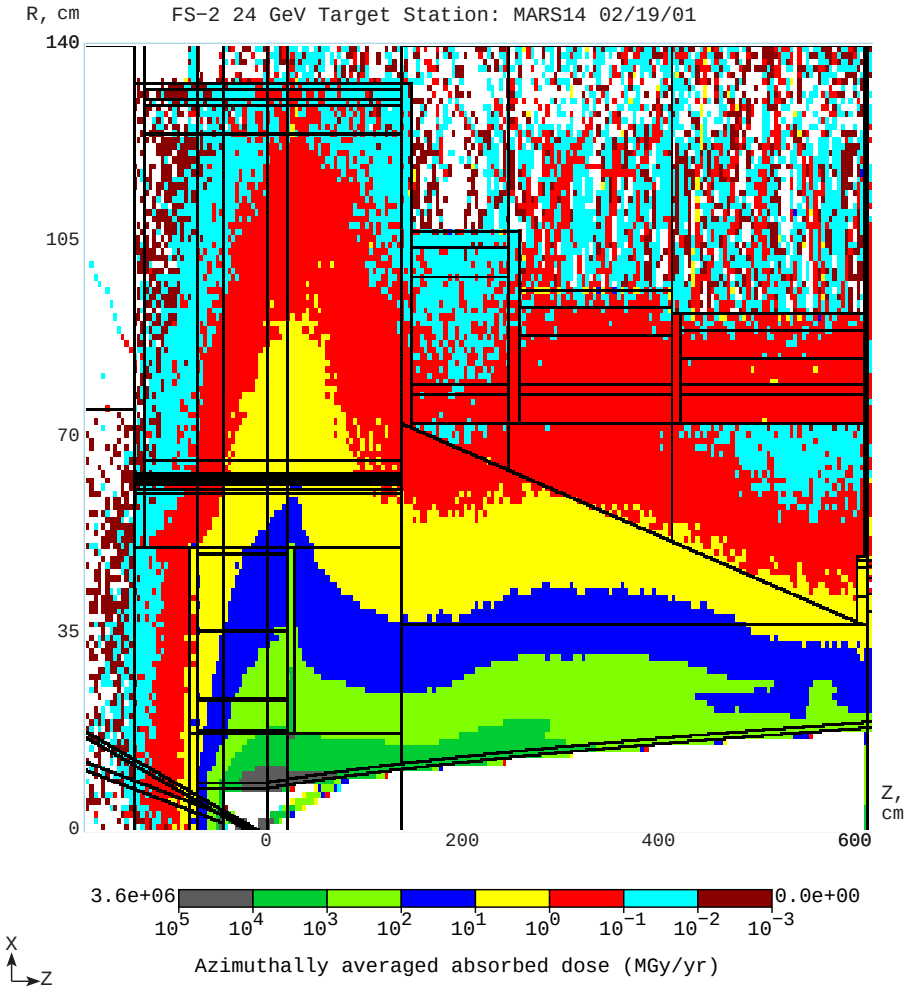

Figure 4: Absorbed radiation dose per year of 2×10^7 s and a 1-MW proton beam in the target system for $-2 < z < 6$ m and $r < 1.4$ m [24].

Preliminary studies have also been made of a support facility for the target system [25], including remote handling equipment and hot cells for processing the activated mercury. Figure 5 sketches the overall concept of the support facility.

Table 1: Estimated lifetime against radiation damage for key components of the target system [21].

Component	Radius (cm)	Dose/yr (Grays/2×10^7 s)	Max allowed Dose (Grays)	1 MW Life (years)	4 MW life (years)
Inner shielding	7.5	5×10^{10}	10^{12}	20	5
Hg containment	18	10^9	10^{11}	100	25
Hollow conductor coil	18	10^9	10^{11}	100	25
Superconducting coil	65	5×10^6	10^8	20	5

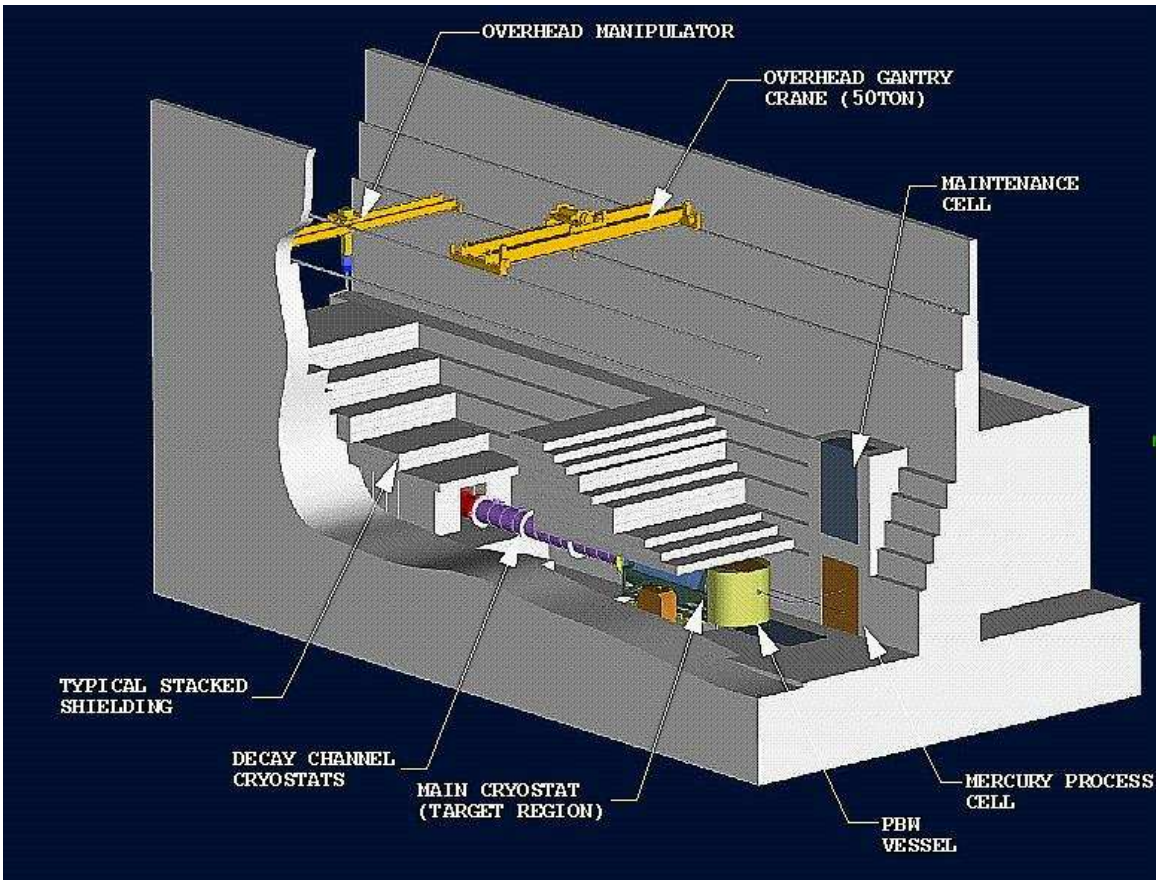

Figure 5: Concept of the target system support facility [25].

1.2 Simulations of Beam + Jet + Magnetic Field

The simulations and studies of the high-power target system described in the preceeding section involved reasonably straightforward extrapolation of the experience of the high-energy and nuclear physics community.

However, there are two key issues related to the proposed use of a liquid jet target which appear to be beyond the present state of the art in simulations:

- To what extent will the jet disperse due to rapid energy deposition by an intense proton pulse?
- To what extent will magnetic forces perturb the flow of the jet into the magnet and affect the possible dispersal of the jet by the beam?

Simple analytic models [26, 27] suggest cautious optimism that the beam-jet-magnet interaction is benign enough to be the basis of a production facility. Yet, there is clear need for more detailed simulation, and for experimental validation of our understanding.

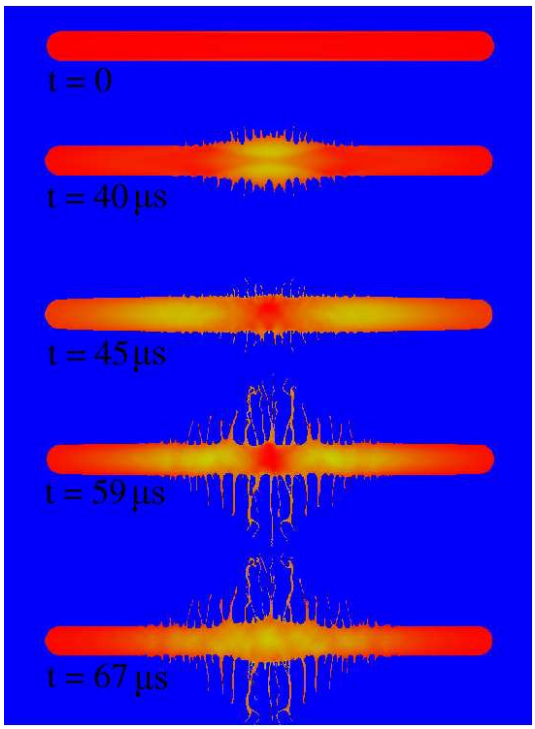

Figure 6: FronTier simulation of a 1-cm-diameter mercury jet in zero magnetic field subject to instantaneous energy deposition at time $t = 0$ with a Gaussian spatial profile peaked at 100 J/gm [30, 31]. A one-phase liquid equation of state was used for mercury.

We have developed an MHD extension of FronTier, a compressible hydrodynamics code for free surface fluids, and performed numerical simulations of hydro and MHD effects in the mercury jet target. In [29], we made some analytical estimates and studies the evolution of

conducting liquid jets and the mercury target entering a strong nonuniform magnetic field. We studied numerically the interaction of the mercury jet with a proton pulse in [30, 31]. The surface instabilities due to the interaction of shock/pressure waves with the jet surface rapidly grow in the absence of a magnetic field and lead to the jet breakup (see Figure 6). When a magnetic field is included in the simulation, it appears that the breakup of the mercury jet is suppressed by the magnetic "pressure" on the conducting liquid, as shown in Fig. 7. We would like to emphasize that the 2D approximation used in the MHD simulations is not accurate after jet surface deformations become large. Currently, we have been working on 3D numerical simulation of the MHD stabilizing phenomena.

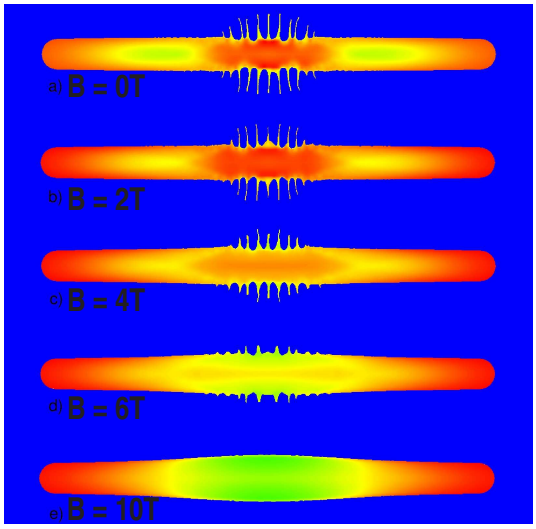

Figure 7: FronTier simulations of a mercury jet at time $t = 50$ μsec after initial energy deposition as in Fig. 6, but immersed in various magnetic field parallel to the jet axis [30, 31].

The time scale of the numerically computed growth of surface instabilities shown in Figures 6 and 7 is smaller compared to experimental data. We explain this discrepancy by the use of a one-phase liquid equation of state for mercury in numerical simulations. The strength of rarefaction waves in the mercury target due to the proton energy deposition significantly exceeds the mercury cavitation threshold. The reduction of the speed of sound in a liquid that occurs shortly after a pulse of energy is deposited [28] strongly influences the wave dynamics in the jet. Therefore the modeling of cavitation and liquid properties under extreme thermodynamic conditions is essential for obtaining accurate predictions based on numerical simulations. We have developed a homogeneous two-phase equation of state for modeling properties of fluids in the presence of cavitation bubbles and incorporated the EOS in the FronTier code [31]. We have performed numerical simulations of the mercury thimble experiments described in section 1.3.3, and obtained a good agreement of the thimble evolution time scale with experimental data. The results are shown in Figures 8 and 9. We have been working on the improvement of the cavitation modeling in the FronTier code by using both the direct tracking of cavitation bubble surfaces and more accurate homogeneous equation of state models.

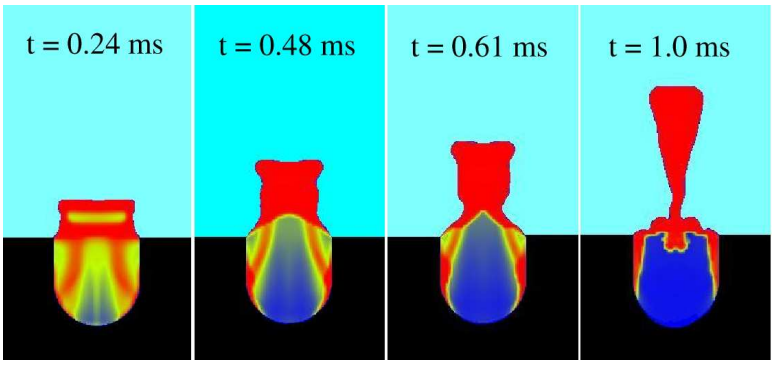

Figure 8: Numerical simulation of the mercury splash in the thimble using the two-phase equation of state for mercury [31].

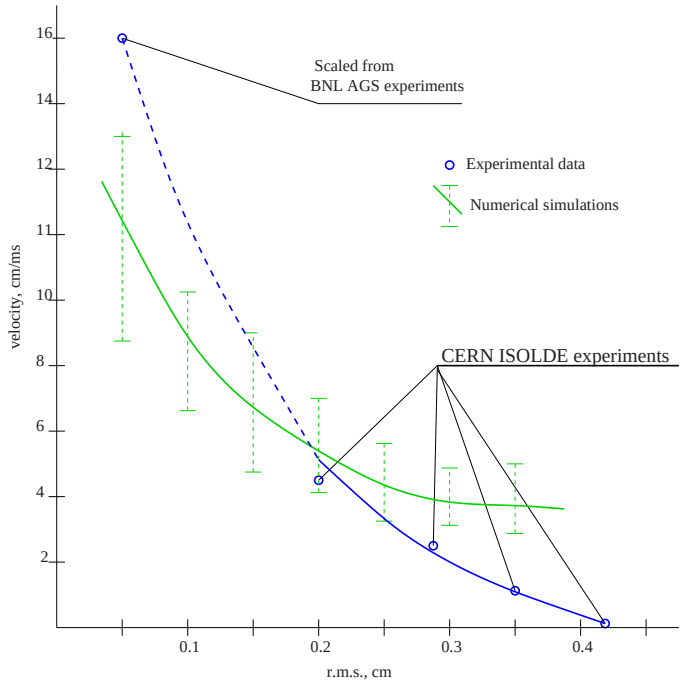

Figure 9: Velocity of the mercury splash in the thimble as a function of the r.m.s. spot size of the beam [31]. The ISOLDE data are from pulses of 1.7×10^{13} protons of 1.4 GeV, while the AGS data is from a pulse of 3.8×10^{12} protons of 24 GeV.

The magnetic pressure is also expected to suppress the breakup of the jet caused by surface tension (Rayleigh [33]) instabilities [34].

Thus, it is very encouraging that the magnetic field, whose original purpose was to enhance the yield of useful secondary particles from the target, also serves to stabilize the operation of a liquid target.

1.3 Results of R&D to Date

The concerns as to the viability of high-power targets for use at a neutrino factory or muon collider have led to an R&D program of international scope. The present proposal seeks to enhance the collaboration between Japan and the USA in these efforts.

The targetry activities in the USA are largely focused on the experiment E-951 [35] at Brookhaven National Laboratory. Activity in Europe has been primarily at the CERN/ISOLDE facility [36] and at the Grenoble High Field Magnet Laboratory [37]. Activity in Japan has largely been in the context of conceptual studies for targets for future neutrino beams [2] and for muon storage rings [5].

Here, we briefly survey some of the results of this ongoing R&D program

1.3.1 Qualification of Materials for Vacuum Windows

Before performing studies of the interaction with mercury targets with a proton beam, it was necessary to qualify the windows of the mercury containment vessel against possible beam-induced failure. Therefore, candidate windows of aluminum, inconel 708, havar (another high-performance steel alloy) and the titanium alloy Ti90Al6V4 were exposed to 100-ns-long pulses of up to 5×10^{12} 24-GeV proton at the BNL AGS.

Pairs of windows were mounted on each face of a double-sided Conflat flange, and the enclosed volume was evacuated. A view of the window test setup is shown in Fig. 10a.

The primary measure of window reliability was that the window-pair unit held vacuum after exposure to the proton beam. All of the candidate windows passed this test.

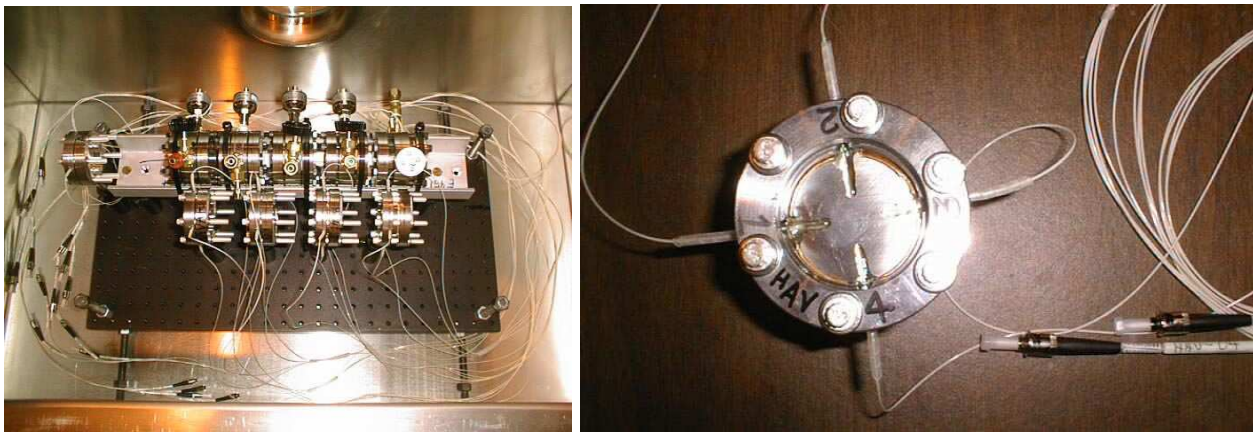

Figure 10: The E951 window qualification setup (left), and a havar window instrumented with four fiberoptic strain sensors (right).

To obtain additional information as to window performance when struck by the proton beam, many of the windows were instrumented with four fiberoptic strain sensors [38]. This technology was chosen because of its immunity to rf interference created by the proton pulses, and because of their frequency response up to about 500 kHz. The construction of the strain sensors in shown in Fig. 11, and their arrangement on a havar window is shown in Fig. 10b.

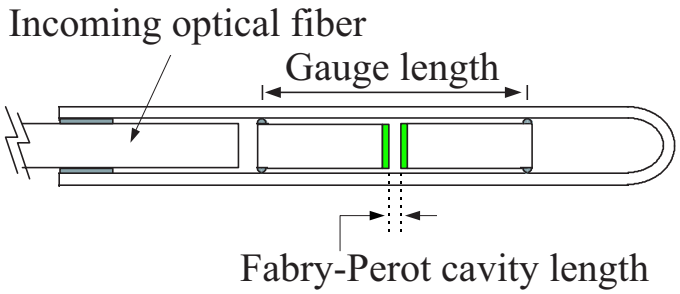

Figure 11: Construction of the Fabry-Perot fiberoptic strain sensors.

Figure 12 shows a comparison between the observed strain in an aluminum window, and an ANSYS model calculation [39, 40]. There is reasonable agreement between data and simulation for both the lower frequency radial strain waves and the high frequency axial waves in the thin windows.

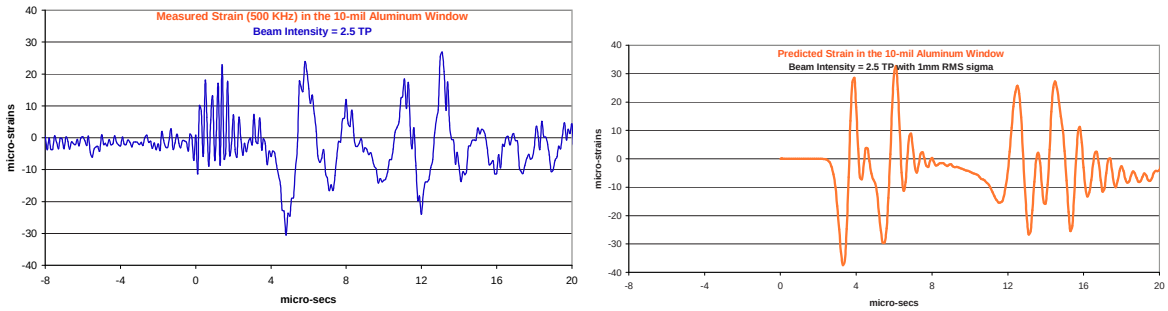

Figure 12: Comparison with observed transient strains in an aluminum window (left) with ANSYS calculations (right) [39, 40].

1.3.2 Studies of Carbon Targets

Carbon is probably the best candidate material for a passive solid target in a high-power application because it retains its mechanical integrity to very high temperature, and because the yield of secondary particles per power absorbed in the target (in contrast to yield per beam power) is higher than for high-Z materials.

Two types of studies of carbon targets have been conducted in the context of BNL experiment E951: the possible advantage of carbon-carbon composites, and the possible suppression of carbon sublimation by operation in a helium atmosphere.

The amplitude of the pressure waves induced in a target by an intense proton pulse is proportional to the coefficient of thermal expansion, according to the simple model that the energy deposited by the beam quickly raises the target temperature, which causes a rapid expansion resulting in the propagation of pressure waves.

Graphite fibers have a very nonisotropic coefficient of thermal expansion. Indeed, the axial coefficient is very small and slightly negative. Certain so-called carbon-carbon composites are manufactured with a 3-dimensional weave designed to provide a near-zero, essentially isotropic coefficient of thermal expansion. If this desirable behavior holds in the presence of energy deposited by a proton beam, the carbon-carbon targets could be largely immune to effects of beam-induced pressure waves.

Beam tests [40, 41] of an ATJ graphite rod (typical of those used in nuclear reactors) and of a low-expansion coefficient carbon-carbon composite indicated that the strains were a factor of five smaller in the latter material, as shown in Fig. 13.

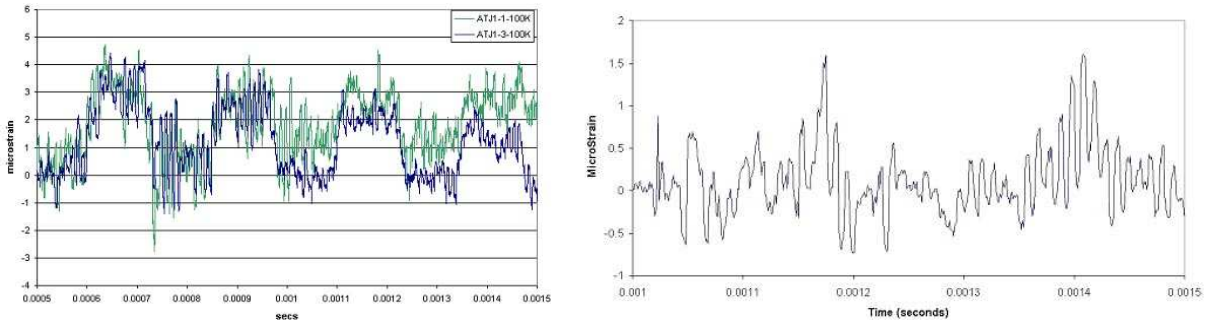

Figure 13: Strains measured in graphite targets exposed to 24-GeV proton pulses. Left: ATJ graphite; right: a carbon-carbon composite [40, 41].

To maintain good collection of low-energy secondary particles from a carbon target, the target should not be in mechanical contact with any other structure such as a cooling unit. That is, radiation cooling should be used. This leads to operation at very high temperatures, perhaps 2400C in case of a 4-MW proton beam. If the carbon target were operated in vacuum, its lifetime against sublimation at that temperature would be only a day or two.

It is anticipated that if the carbon target is operated in helium at one atmosphere, the rate of sublimation will be reduced by at least two orders of magnitude [42]. Studies are underway at Oak Ridge National Laboratory to confirm this desirable behavior [43].

1.4 Studies of the Effects of Radiation Damage on High-Performance Alloys

Another aspect of our studies of solid targets is measurements of the effect of radiation damage on the strength and on the thermal expansion coefficient of various high-performance alloys. As noted in the previous section, materials with low coefficients of thermal expansion, such as carbon-carbon composites, SuperInvar, and a new titanium alloy developed by Toyota Motors [44], will have enhanced ability to survive the pressure waves induced by the rapid energy deposition of a pulsed proton beam.

Results from a first set of studies at the Brookhaven Linac Isotope Production Facility (BLIP), shown in Fig. 14, revealed that the SuperInvar alloy suffers a substantial increase in its coefficient of thermal expansion at relatively low radiation doses [45]. Its strength increases slightly with radiation dose, as is typical for metals.

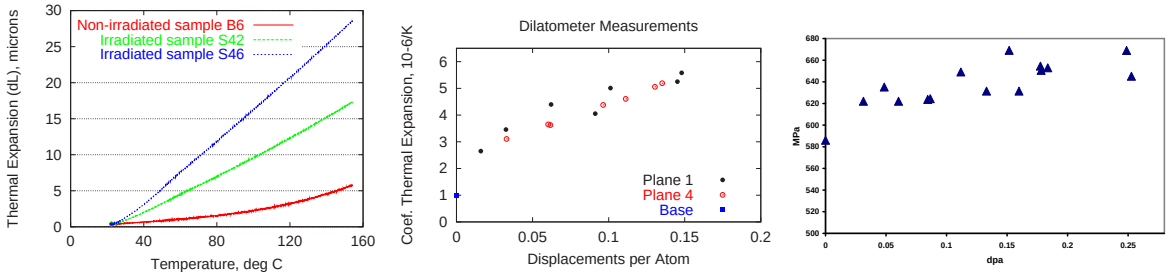

Figure 14: a) The thermal expansion of SuperInvar as a function of temperature, before and after irradiation in the BLIP Facility. b) The coefficient of thermal expansion of SuperInvar at 30°C as a function of radiation dose. c) The yield strength of SuperInvar as a function of radiation dose. From [45].

Because of the striking deterioration of the desirable properties of SuperInvar with radiation dose, considerable interest has arisen in performing similar studies for other alloys [46]. A second round of studies in now in progress [47] of AlBeMet, a carbon-carbon composite, IG-43 graphite, titanium Ti-6Al-4V, the Toyota titanium alloy, and Vascomax 350.

1.4.1 Beam Studies of a Passive Mercury Target

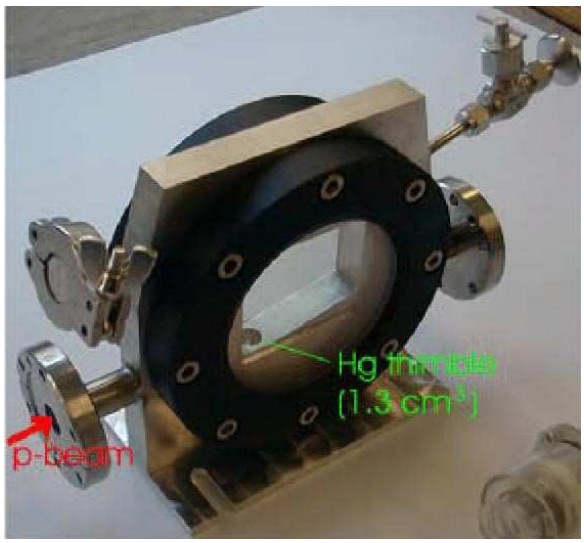

Figure 15: View of the passive mercury target. The mercury was contained in the "thimble" = cylindrical well visible at the left side of the circular viewport. The proton beam entered from the left through the Conflat flange.

The first studies of E951 of the interaction of a proton beam with a mercury target were performed with a passive "thimble" of mercury, 1.0 cm in diameter, 1.5 cm high, shown in Fig. 15. High-speed shadow photography of the interaction of the mercury "thimble" with proton beams at BNL and at CERN/ISOLDE [48, 49, 50, 51] showed that the beam

disperses the mercury with velocities proportional to the total energy in the beam pulse, an example of which is shown in Fig. 16. The velocities ranged from 10 to 50 m/sec in the studies performed, so that the impact of the mercury droplets with the walls and windows of the containment vessel was nondestructive.

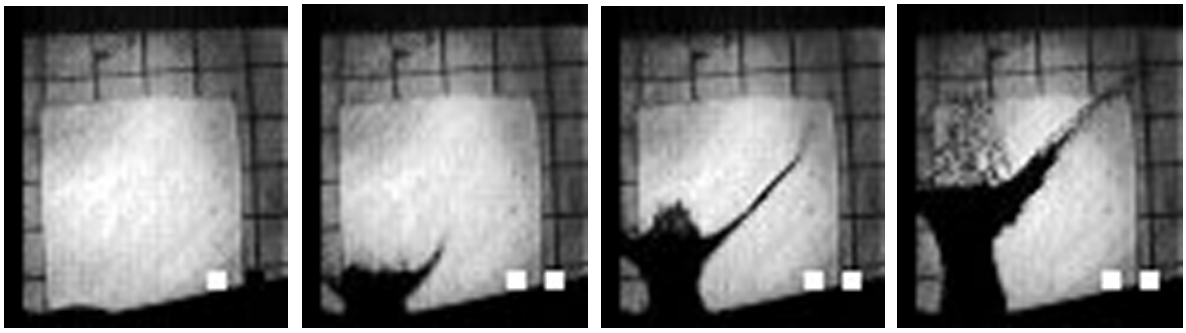

Figure 16: Exposures of 25 μs at t = 0, 0.5, 1.6, 3.4 msec after a mercury "thimble" 1.0 cm in diameter and 1.5 cm deep was struck by a pulse of 2×10^{12} 24-GeV protons.

At the CERN/ISOLDE facility it was possible to send a pair of proton pulses into the "thimble" with intervals between the pulses ranging from 0.5 to 8 μsec. The dispersal velocity of the mercury in the case of two pulses was greater than that for one pulse provided that the time interval between the pulses was less than 3 μsec [51].

1.4.2 Beam Studies of a Mercury Jet

A free mercury jet, 1 cm in diameter with velocity 2.5 m/s, was constructed as in Fig. 17 and exposed to 24-GeV proton pulses at BNL [49, 50, 51]. High-speed photography (Fig. 18) showed that the velocity of dispersal of the mercury was about one half that in the case of the "thimble" target, for the same proton pulse intensity. The higher dispersal velocity in the case of the "thimble" occurs because the reflections of the pressure wave off the steel wall of the thimble are stronger than those off the free surface of the mercury jet.

An important qualitative result is that the dispersal of the mercury by the proton beam was confined to the region of overlap of the beam with the jet. The pressure waves inside the mercury jet did not appear to propagate along the jet. This suggests that the nozzle which produces the mercury jet can be located close to the interaction region without being damaged by the pressure waves in the mercury.

Another noteworthy result, obtained by photography with 1-μsec between frames, is that the visible onset of the dispersal of the mercury occurred about 40 μsec after the proton pulse. This contrasts with a time of only 3-4 μsec for a sound wave to reach the surface of the jet, if the speed of sound is the nominal 1500 m/sec. This results supports the interpretation of a study of proton beam interactions with a closed vessel of mercury [28] that the speed of sound in mercury is temporarily reduced after interacting with an intense pulse of protons.

In the beam studies conducted to date, the energy deposition was insufficient to raise the temperature of the mercury to its boiling point. However, pulses of order 10^{14} protons, as

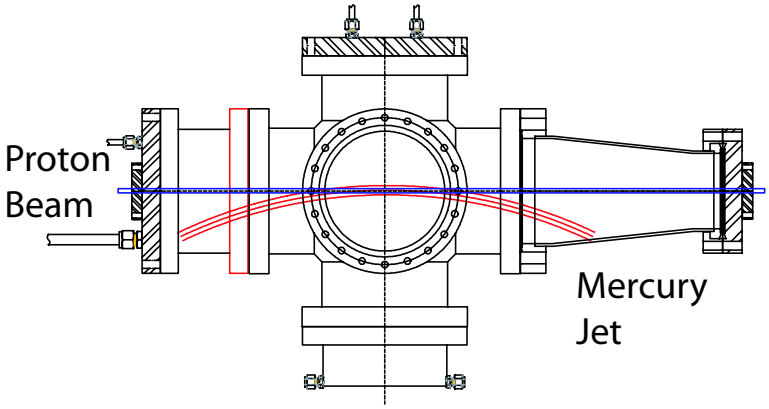

Figure 17: Side view of the apparatus to produce a 1-cm diameter mercury jet with velocity 2.5 m/s whose trajectory overlapped with the BNL proton beam for about 10 cm.

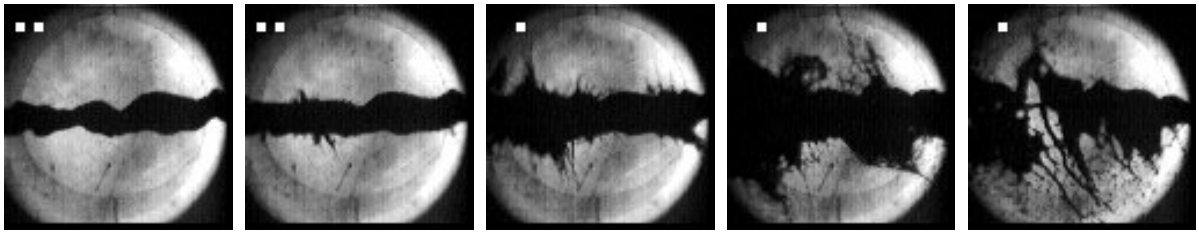

Figure 18: Exposures of 25 μs at t = 0, 0.75, 2, 7, 18 msec after a 1-cm diameter mercury jet was struck by a pulse of 2×10^{12} 24-GeV protons.

foreseen in 4-MW beams, would be sufficient to do so. This will, in general, provide additional means of dispersal of the mercury, which is being studied via simulations at present [52], but deserves further laboratory study as well.

1.4.3 Interaction of a Mercury Jet with a 20-T Magnetic Field

Studies of a mercury jet of 4-mm diameter and 12-m/sec velocity have been made in magnetic fields up to 20 T at the Grenoble High Field Magnet Laboratory, with the setup sketched in Fig. 19 [51]. The axis of the jet could be tilted with respect to the axis of the magnet between 0 and 100 mrad.

Based on high-speed shadow photography, as shown in Fig. 20, a field of 20-T stabilized the surface perturbations of the jet, a very desirable result. The dispersal of the jet by a proton beam may also be reduced or suppressed by a strong magnetic field.

The 4-mm-diameter jet was able to enter the magnetic field, both at 0 and 100 mrad to the magnetic axis, without noticeable deflection, although the overall jet velocity was reduced somewhat (as expected from eddy current effects [27]). Since the deflections due eddy-currents grow as the square of the jet diameter, they will be about six times stronger in the case of a 1-cm-diameter jet, which deserves further study.

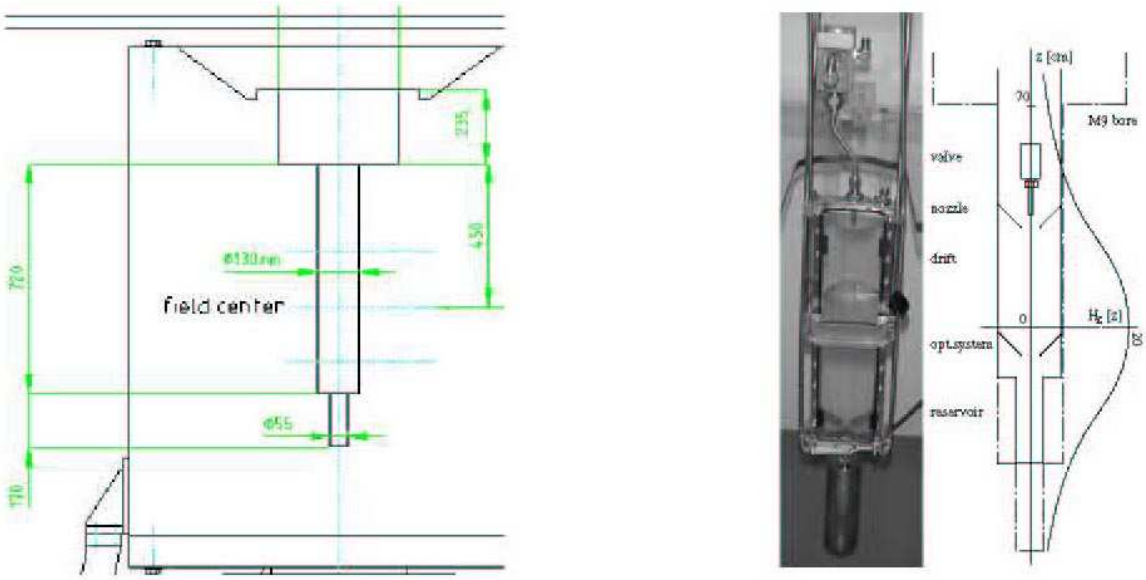

Figure 19: Left: Vertical section through the 20-T, 13-cm-diameter bore of the M9 solenoid magnet at the Grenoble High Field Magnet Laboratory [37]. Right: The apparatus inserted into the M9 magnet bore that included a mercury jet and a mirror system to permit high-speed shadow photography [51].

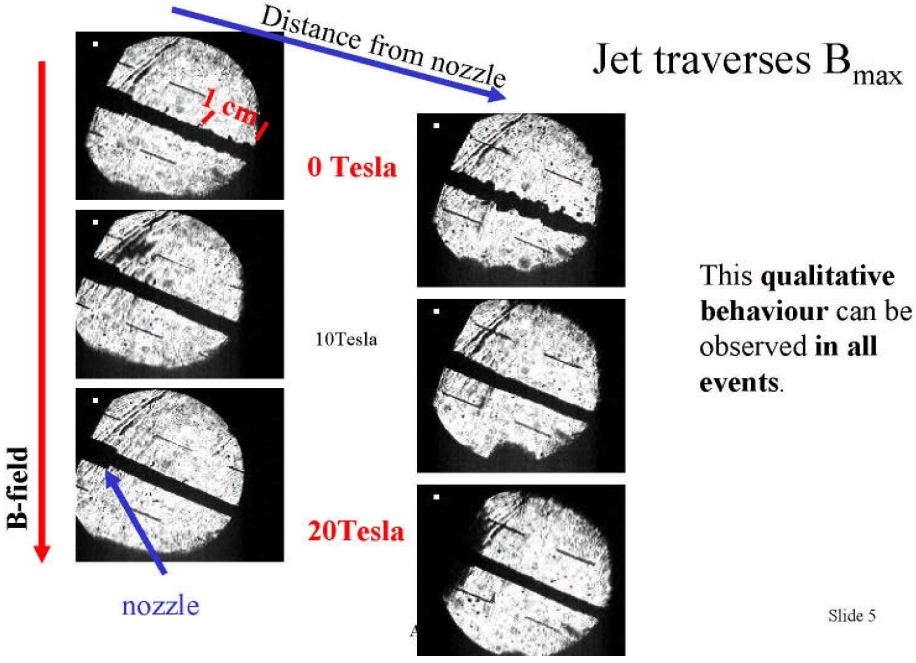

Figure 20: High-speed shadow photographs of a mercury jet of 4-mm-diameter and 12 m/sec velocity in magnetic fields of 0, 10 and 20 T [51]

2 Proposed Studies of Beam + Mercury Jet + Magnetic Field

The studies of components of a mercury jet target system, described briefly in sec. 1.3, are very encouraging, and suggest that a system test in a near-prototype configuration is the next step for high-power targetry R&D.

Keys results from the mercury target studies to date include:

- A mercury jet is dispersed by an intense proton pulse in a nondestructive manner, at low velocities proportional to the pulse intensity.
- The region of dispersal of the mercury jet is largely limited to the region of overlap with the proton beam. The pressure waves that cause the dispersal do not appear to propagate along the axis of the jet.
- The onset of dispersal is delayed with respect to the proton pulse by a time which suggests that the velocity of sound in mercury is temporarily reduced by the energy deposition of the proton pulse.
- A strong magnetic field stabilizes the surface perturbations of the jet.
- Small-diameter jets can enter a strong magnetic field without significant deflection, although the longitudinal velocity of the jet is reduced.

Based on the above results, we propose a second round of high-power target studies whose primary goal is:

▷ A proof-of-principle demonstration of a mercury jet target in a strong solenoid magnet with proton pulses appropriate for a multimegawatt source.

Subsidiary goals in support of the primary goal include:

▷ Studies of a 1-cm-diameter mercury jet entering a 15-T solenoid magnet at various velocities and angles.

▷ Studies of dispersal of the mercury jet by pulses due to both pressure waves and vaporization.

▷ Studies of magnetic suppression of the dispersal of mercury by proton pulses.

To realize these goals, we propose that a mercury target station with a 15-T solenoid magnet be constructed in a 24-GeV fast-extracted beam at CERN. Key features of this target station include:

⋆ Use of a 1-cm-diameter mercury jet the overlaps with the proton beam for at least 30 cm.

⋆ Use of a 15-T, 15-cm-diameter warm-bore magnet, whose axis can be tilted with respect to the beam/jet axis by 0-150 mrad.

- ⋆ Use of pulses of 24-GeV protons of up to 4×10^{12} each, with the option to extract a train of up to all 8 pulses from the CERN PS.

An important restriction to the goals of the proof-of principle demonstration is that it does not address issues of long-term survival of the target system. Rather, it will demonstrate full functionality of the system on a pulse-by-pulse basis, with a total of only 100-200 beam pulses.

2.1 The 15-T Pulsed Magnet Test Facility

The essential concept of the present proposal is the combination of an intense proton beam, a mercury jet target, and a high-field solenoid magnet in a single facility.

The solenoid magnet for this facility is a cost driver, so careful consideration must be given to its specifications: field strength, choice of magnet technology, including DC *vs.* pulsed operation.

As shown in Fig. 3b, the yield of low-energy secondary pions and muons improves with the field strength up to 20 T in a suitably designed solenoid-magnet capture system. However, the technology of large superconducting magnets is presently limited to about 14 T, so a 20-T magnet capture solenoid would be a hybrid system with a 14-T superconducting coil and a 6-T water-cooled copper coil [21]. The small gain in secondary particle yield in a 20-T system compared to a 14-T system may not justify the extra expense of a hybrid technology solution.

Hence, we consider that 15-T operation is a suitable goal for the proof-of-principle target and capture system.

Further, the proof-of-principle demonstration that we desire to perform is not one of magnet technology, but rather of the operation of a system of magnet + mercury jet + beam. We propose to use the most cost effective technology capable of providing 15 T over a warm bore 1 m long and 15 cm in diameter during the proton pulses.

The strength of the interaction of the magnetic field B with the mercury jet scales as B^2 for most effects [27]. Hence, use of a 5-T magnet for the proposed tests would imply an order-of-magnitude extrapolation beyond the data collected to reach the regime appropriate for a production target facility. We consider that a "proof-of-principle" demonstration has not been made if an order-of-magnitude extrapolation remains. Use of a 10-T magnetic field would leave a factor of two extrapolation; only if budget realities exclude the construction of a 15-T magnet, would we consider this option. In sum, 15-T is the appropriate magnetic field strength for the proposed proof-of-principle demonstration experiment.

Since the scope of the demonstration is to validate the high-power target concept on a pulse-by-pulse basis, the magnet for this demonstration could be a pulsed magnet. (Of course, a 15-T pulsed magnet is not a realistic option for an eventual production facility).

These considerations have led us to propose use of a 15-T pulsed magnet system whose design equalizes the costs of the three main system components (at $\approx$ \$400k each):

1. The pulsed magnet coils.

2. The magnet cooling system.

3. The magnet power supply.

Some details of these subsystems will be given in the following subsections.

Diagnostics of system performance will be primarily optical, based on high-speed shadow photography as described in secs. 1.3.3-1.3.5. Details of the optical instrumentation would be similar to that sketched in Fig. 19 (although the magnet axis will be horizontal in the proposed studies, in contrast to the vertical axis of the Grenoble M9 magnet).

2.1.1 Conceptual Design of the 15-T Liquid-Nitrogen-Precooled Pulsed Magnet

A sketch of a horizontal section through the proposed 15-T pulsed magnet is shown in Fig. 21. The magnet consists of three nested coils wound from solid, rectangular copper conductor, with axial cooling channels between (and outside of) the three coils [53].

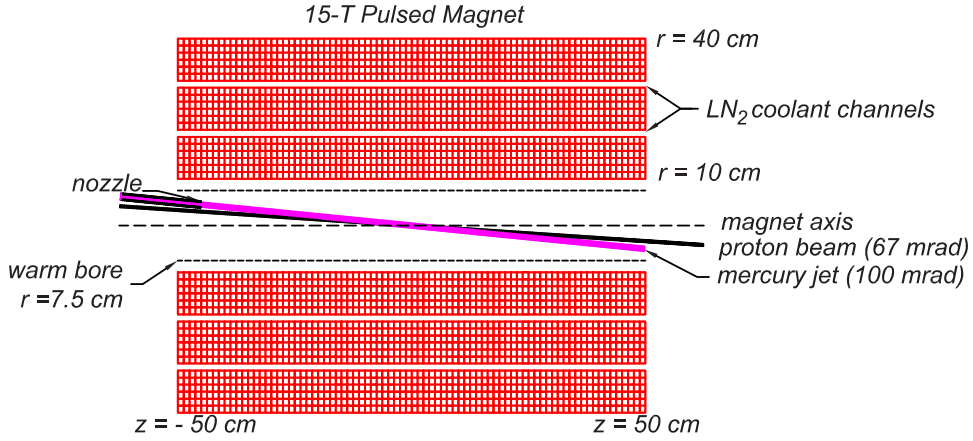

Figure 21: A horizontal section through the proposed 15-T pulsed magnet, which has a 15-cm-diameter warm bore inside which the proton beam and mercury jet overlap at angles up to 100 mrad to the magnetic axis [53].

To reduce the power consumption, and hence the size of the coil, cooling system and power supply, the coils are operated at cryogenic temperatures. Figure 22 shows how the resistivity and heat capacity of copper vary with temperature, which indicates that it is advantageous to operate a copper magnet at temperatures as low as about 30K.

Between pulses, the magnet is cooled by injection of liquid nitrogen at a controlled rate such that the output from the cooling channels is essentially all nitrogen gas. A pump on the outlet side permits the temperature of the liquid nitrogen to drop to 70K, the desired operating temperature of the magnet. Just prior to pulsing the magnet, the flow of liquid nitrogen is halted, and all liquid pumped out of the magnet to minimize activation of nitrogen by the proton beam.

Figure 23 shows the (relative) field strength as a function of position along the axis of the 15-T pulsed magnet. In a region of ± 1 interaction length (± 15 cm) the field varies by only 2.5% (*i.e.*, 1% rms variation).

The time dependence of several parameters of the 15-T magnet during a pulse are shown in Fig. 24. The current (which is proportional to the magnetic field) takes about 10 sec to

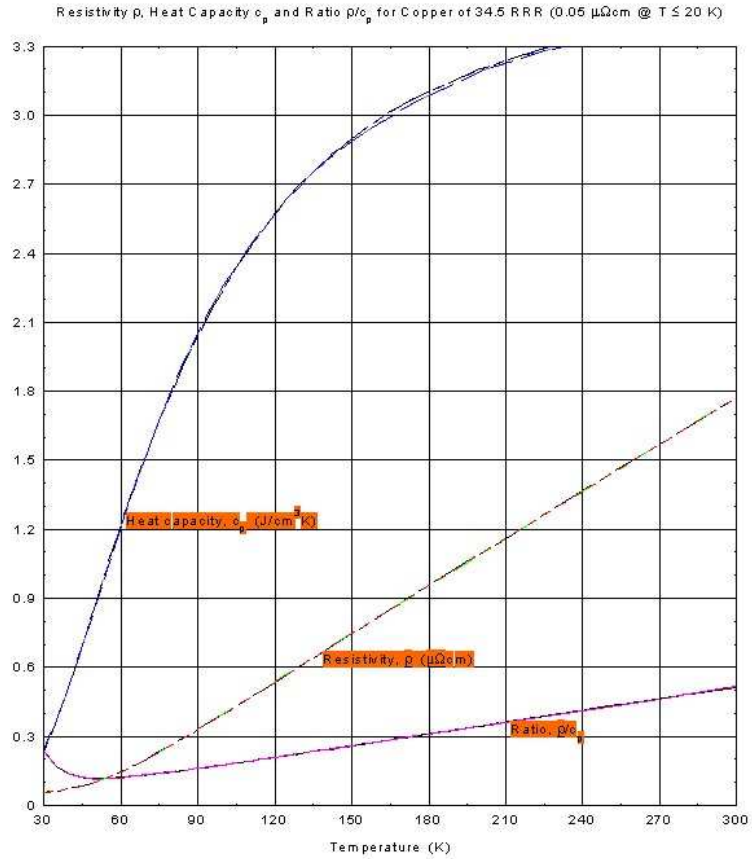

Figure 22: The resistivity and heat capacity of copper as a function of temperature [53].

ramp up to 7200 Amps, and is brought down in about 5 sec. About 20 MJ of energy is deposited in the magnet due to Joule heating, in consequence of which its temperature rises by 30K.

The time needed to remove the 20 MJ of Joule heating determines the operational cycle time of the system. This is expected to be at least 30 min per pulse at 15 T.

2.1.2 The 15-T Pulsed Magnet Coil Package

Figure 25 shows two assembly drawings of the 15-T coil package and cryostat from a detailed engineering study [54]. The full drawing set for this magnet can be viewed at [55].

The current leads to each of the three coils are fed through the cryostat to permit external connections to be made separately, permitting operation of the magnet at 5, 10 or 15 T as desired.

The solenoid magnet and its cryostat are presently being fabricated by CVIP Inc.[7] with a subcontract to Everson Tesla[8] for the three coils. A recent status report on the magnet

[7]Cryogenics Vessels Instrumentation & Piping, Inc., Emmaus, PA 18049, www.cvipinc.com
[8]Everson Tesla Inc., Nazareth, PA 18064, http://www.eversontesla.com

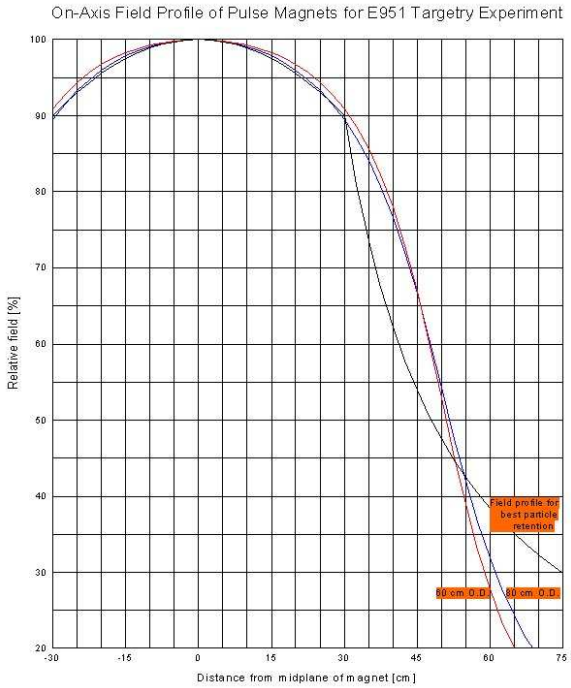

Figure 23: The calculated axial profile of the magnetic field in the 15-T pulsed magnet [53].

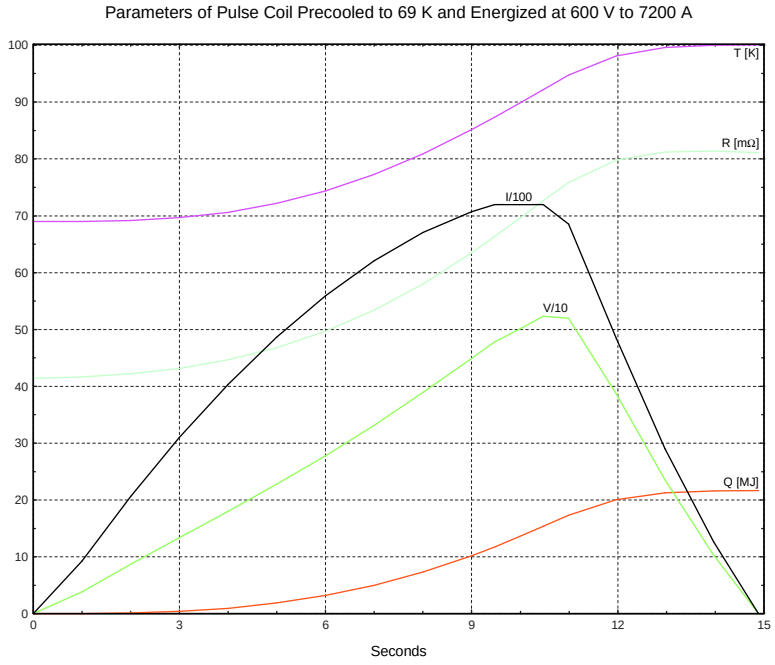

Figure 24: Time dependence in the 15-T pulsed magnet of the temperature T, the current I (with is directly proportional to the magnetic field B), the coil resistance R, the voltage drop V across the coil, and the energy Q deposited in the coil by Joule heating.

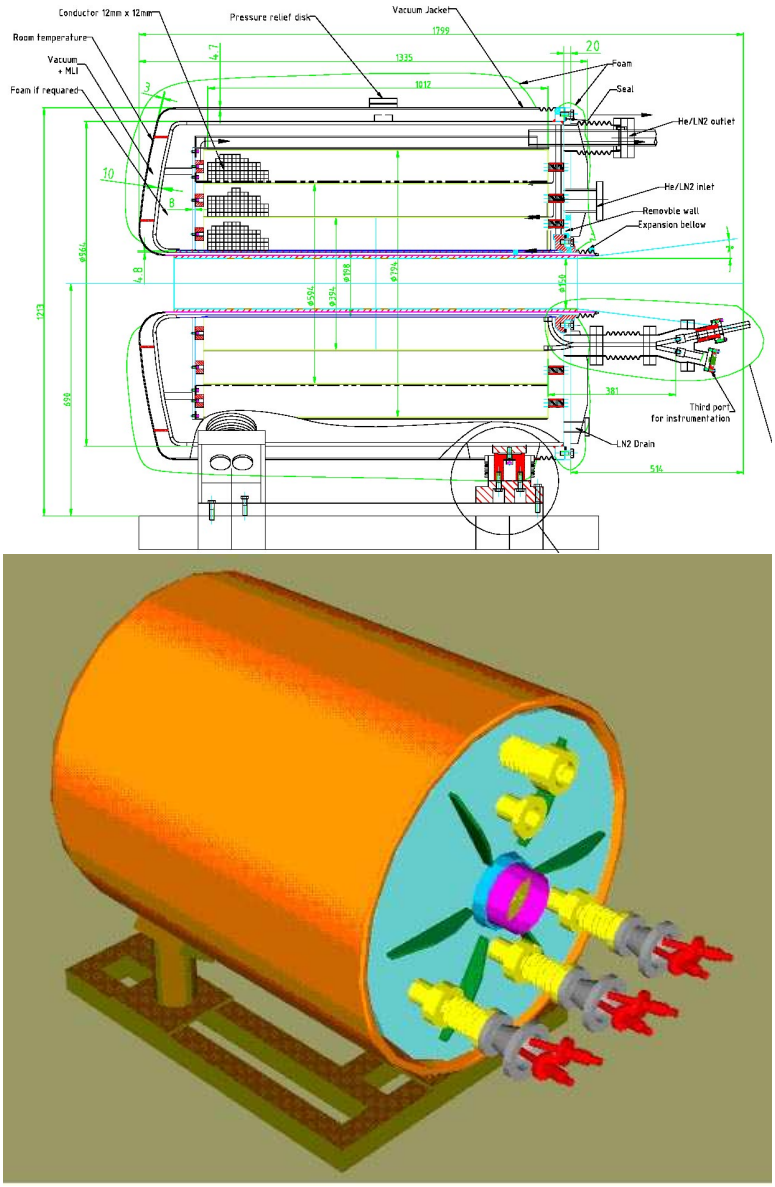

Figure 25: Sketches of the concept of a 15-T, pulsed copper solenoid for use in the prototype target studies [54].

fabrication is [56].

2.1.3 The 15-T Pulsed Magnet Cooling System

Figure 26 sketches the proposed cooling system for the 15-T pulsed magnet. Between pulses of the magnet, liquid nitrogen is delivered from a supply dewar at a rate such that essentially all of the liquid boils before exiting the magnet. This process is assisted by a vacuum pump on the outlet side of the magnet, which also permits the ultimate temperature of the magnet to be 70K (for 0.2 atm pressure).

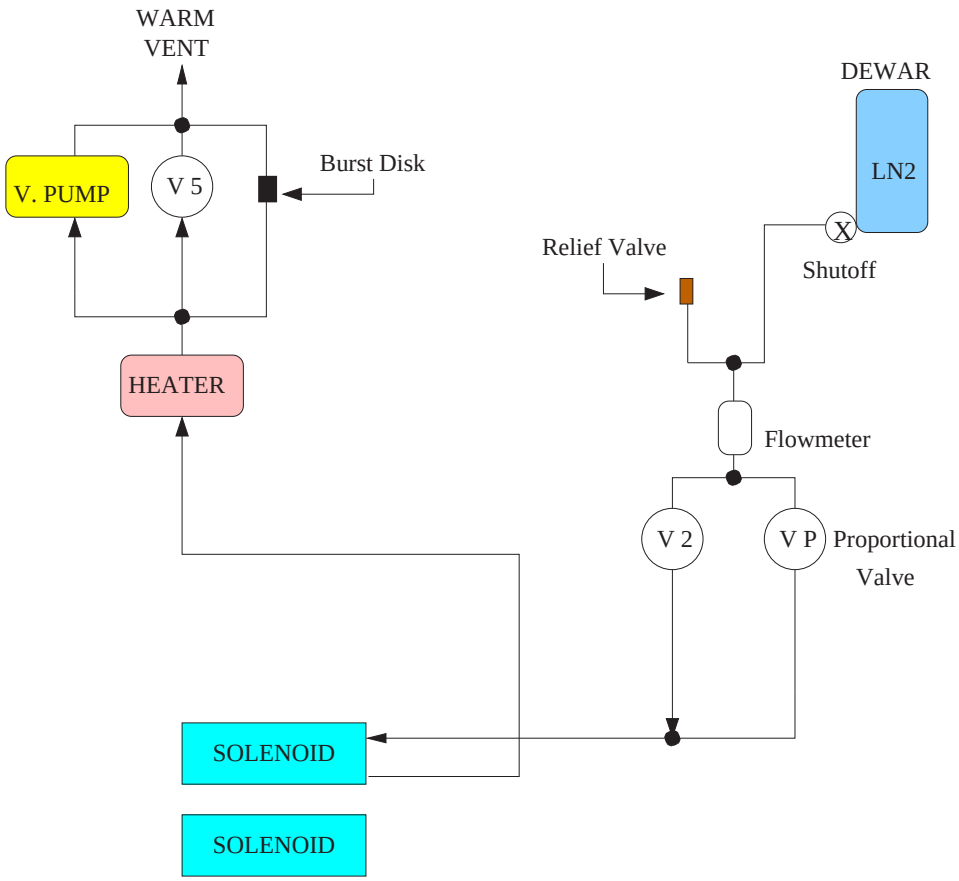

Figure 26: Sketch of the proposed liquid-nitrogen cooling system for the 15-T pulsed solenoid magnet.

To avoid activation of nitrogen by the proton beam, the liquid supply is turned off before a pulse, and the residual liquid pumped out of the magnet.

The time required to cool the magnet down from 100K to 70K after a pulse at 15 T is estimated to be between 30 and 60 min [57].

The cooling of the magnet will result in a discharge of approximately 1000 m^3/hour of nitrogen gas. An exhaust channel to the outside air should will be provided to avoid the hazard of oxygen depletion in the experimental area.

2.1.4 The 15-T Pulsed Magnet Power Supply

Operation of the solenoid at 70K will permit a magnetic field of 15T when excited with a (pulsed) current of 7200 Amps at 600 V (4.32 MVA peak power). The power supply need not be highly regulated; the load is highly inductive (0.5 Henries, 0.04 Ohms).

This requirement is very similar to that of the power converter for the Alice and LHCb experiments, so we propose to purchase a similar system [58].

Because our application is very low duty cycle ($< 1/200$), it may be possible to simplify the design of the Alice/LHCb power converters, resulting in a lower cost.

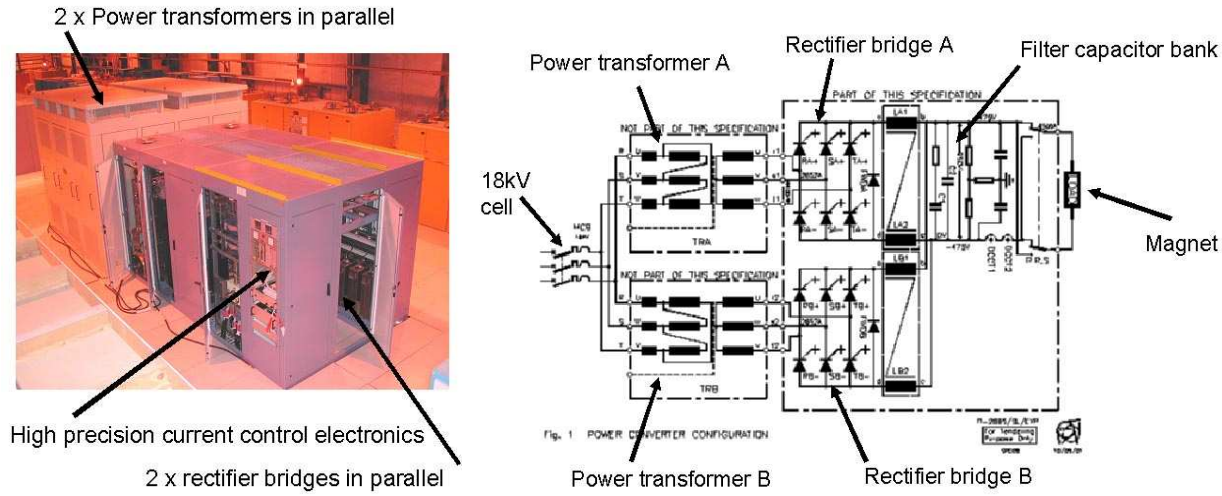

Figure 27: Photo and schematic of the Alice/LHCb power converter whose specifications are well matched to the present requirements of 7200 A at 600 V. From [58].

2.1.5 The Mercury Jet Target and Its Diagnostics

The primary diagnostic of the mercury jet target performance will be optical, as discussed below. In addition, a set of scintillation counters in the vicinity of the magnet will provide a monitor of the relative production of secondary particles for each bunch of the proton bunch train.

The concept of the optical diagnostic is shown in Fig. 28, which is an extension of the system successfully used in our previous studies of mercury jets at BNL, ISOLDE and at the Grenoble High Magnetic Field Laboratory [51].

A 1-cm-diameter jet of mercury will be propelled at 20 m/s by a centrifugal pump. This high velocity is required so that the jet is straight enough over the desired 60-cm-long interaction length with the proton beam. The mercury jet is contained within a stainless steel vessel that protrudes into the 15-cm-diameter warm bore of the solenoid magnet. Beam windows permit the proton beam to enter the mercury containment vessel; the windows located sufficiently far from the proton beam focus that there is no risk of window failure.

Approximately 4 liters (55 kg) of mercury will circulate in the system, with a 2-sec cycle time.

The interaction of the proton beam with the mercury jet will be viewed by a high-speed camera via a folded optical path, with a laser diode as the light source. Two sets of mirrors permit part of the optical field of view to include a region in the interior of the solenoid magnet. The mirror set within the magnet can be moved remotely so that different portions of the mercury jet could be viewed during different proton pulses.

Some details of the diagnostic chamber inside the magnet are sketched in Fig 29.

An option exists to further subdivide the optical path so that two region of the jet within the magnet can be viewed during each proton pulse, as illustrated in Fig. 30. One of the images would be collected from the upstream end of the magnet through an additional optical

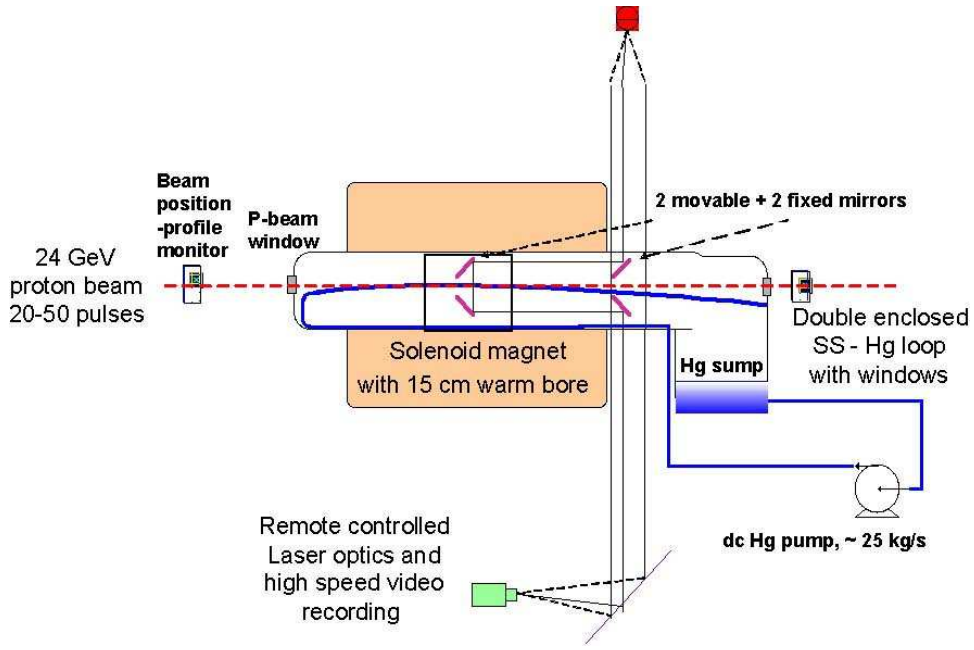

Figure 28: The 20-cm/s, 1-cm-diameter mercury jet flows inside a stainless steel containment vessel with windows for the proton beam and for optical diagnostics. Two sets of mirrors provide a folded optical path to view the mercury jet at the center of the solenoid magnet, where it interacts with the proton beam. A high-speed camera views the mercury jet via shadow photography based on illumination of the jet by a laser diode.

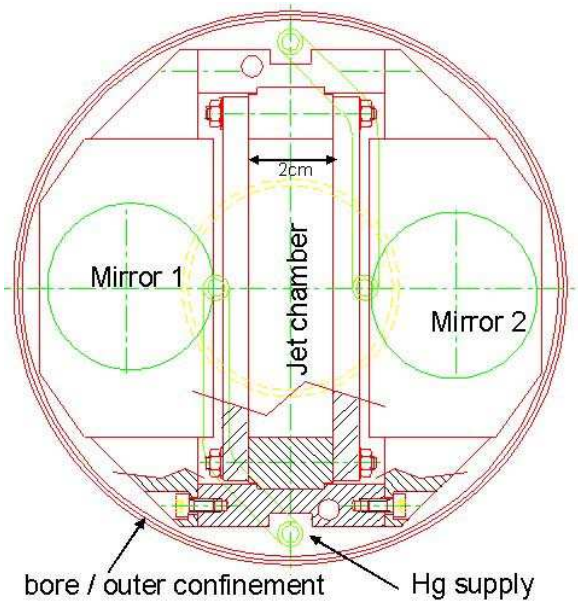

Figure 29: A transverse cross section through the jet-diagnostic chamber as the position of the mirrors that permit a view of the mercury-proton interaction.

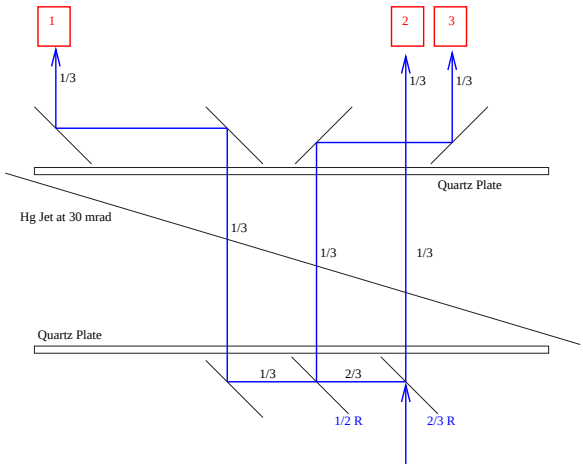

Figure 30: A beam spitter plus 3 additional mirrors would provide the option to view the mercury jet at two positions within the magnet.

window.

2.2 Siting of the Target Test in the CERN nTOF Beamline

The present proposal is for high-power target studies to be conducted in the CERN Neutron Time of Flight (nTOF) beamline, in the TT2A tunnel some 20-40 m upstream of the nTOF target.

- The studies proposed here are to be made using small numbers ($< 1{,}000$ total) of intense 24-GeV proton pulses in the CERN Neutron Time-of-Flight beamline. Of these pulses, only about 40 will be used for studies of the interaction of the proton beam with the mercury jet; the other pulses are for beam tuning.
- A "pulse-on-demand" mode of operation is desired, in which a proton pulse is used at most every few minutes. A higher repetition rate would be useful during beam setup.
- The studies should be carried out in an area suitable for use with a primary proton beam, such at the TT2A tunnel. The small number of beam pulses required will, however, limit the activation of materials to low levels.
- The target system + surrounding 15-T solenoid magnet could occupy as little as 2 m along the beamline. If the solenoid magnet axis is tilted horizontally with respect to the proton beam axis as desired, then the solenoid should be immediately followed by a vertical trim magnet with field integral of 1 T-m.
- The beam should be focusable to a spot of rms radius ≈ 2 mm at the target location.
- The main mode of beam delivery from the CERN PS should be single-turn extraction of up to 4 rf bunches, for a total of 2×10^{13} protons. However, it is desirable to be able to extract any number from 1 to 8 of these bunches during a single turn. A programmable fast-kicker is required for this.

- The mercury jet is to be about 1-cm diameter, flowing at 10-20 m/sec, entirely within a stainless-steel containment vessel (with beam entrance and exit windows of a high-strength alloy). Diagnostics of the beam/jet interaction are primarily optical.
- The pulsed magnet is advantageously operated at about 70K to lower the resistance of its copper coils. A LN_2 storage dewar of at least 6,000 liters is required.
- The magnet requires a special power supply, capable of 4.6 MW peak power.

A suitable location for the proposed studies is the TT2A tunnel that houses the nTOF transfer line [60, 61]. Figure 31 gives an overview of the nTOF beamline, which runs from the PS to the time-of-flight tube underneath the ISR ring. Details of the nTOF line in the TT2A tunnel, just upstream of the nTOF target, are shown in Figs. 32-34.

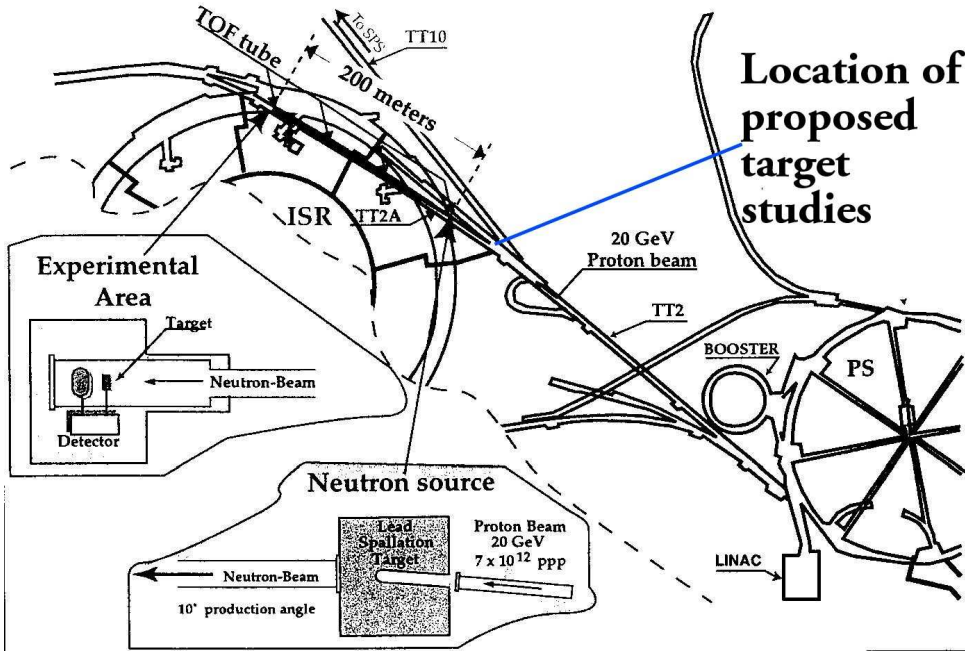

Figure 31: Overview of the nTOF beamline, which resides in the old proton transfer line between the PS and the ISR.

Three options for siting the proposed target test facility at intermediate foci along the nTOF line, some 20-40 m upstream of the nTOF target, were considered in our Letter of Intent [59], as shown in Fig. 34. Photographs of these locations are shown in Figs. 35 and 36.

On further review of these options, it was concluded that the site of option 1 is too congested with equipment, which would become somewhat activated by our experiment.

Figure 37 shows the horizontal and vertical dispersion and spot size as a function of position along the nTOF beamline [60]. To reduce the horizontal spot size to the desired 2 mm (rms), we propose to operate the PS without the longitudinal bunch compression that is standard for the nTOF beamline. This will reduce the horizontal dispersion, and horizontal spot size by about a factor of 2.

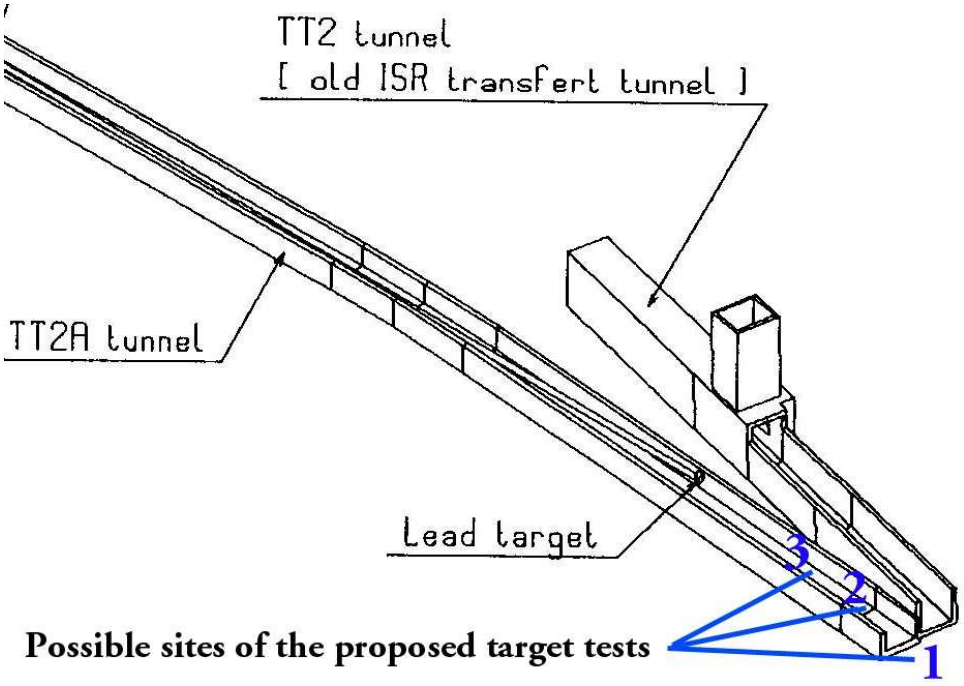

Figure 32: Sketch of the TT2 and TT2A tunnels. Three possible locations for the proposed target test are close to the intersection of the two tunnels. Horizontal and vertical access to these tunnels is via the TT2 tunnel. We now favor option 3, followed by option 2.

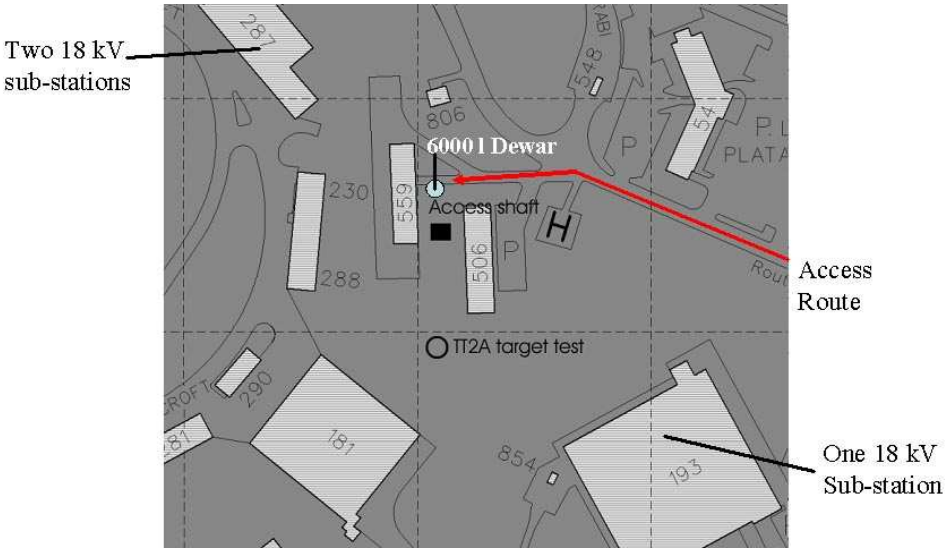

Figure 33: Layout of surface facilities in the vicinity of the proposed target experiment in the TT2A tunnel. A 6,000 l dewar of liquid nitrogen could be placed near the vertical access shaft into the TT2-TT2A tunnels. The AC power for the 4.6 MW power supply could be obtained from substations (cellules) in nearby service buildings.

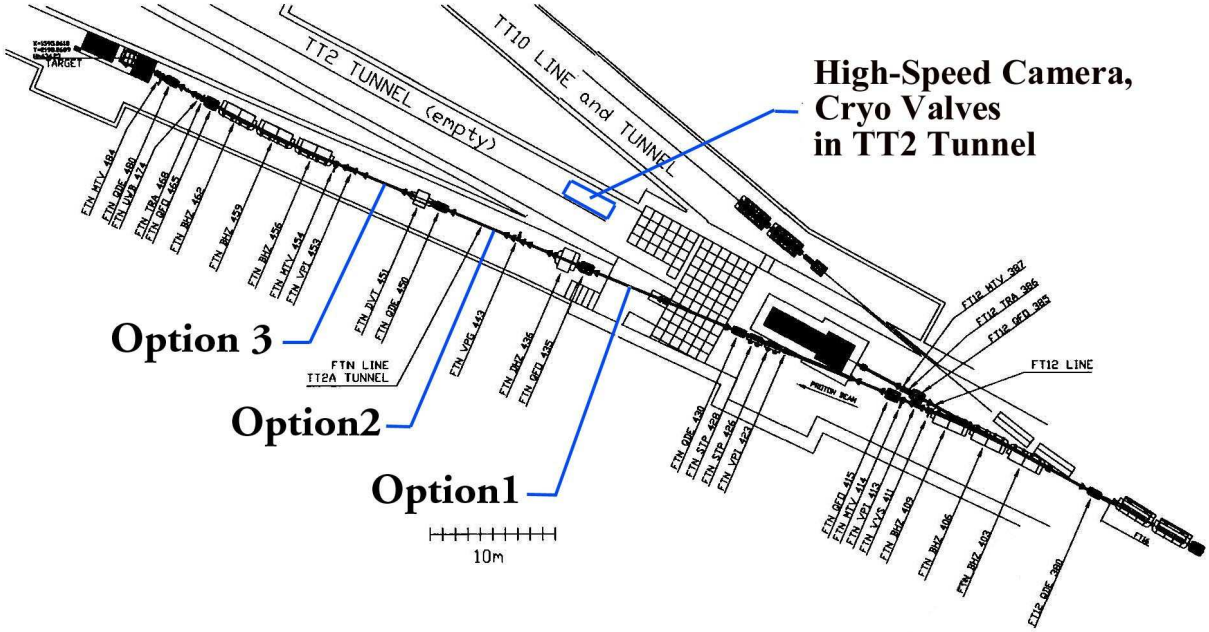

Figure 34: Details of the nTOF beamline in the TT2A tunnel. Three possible locations for the proposed target test facility are shown. The present proposal is to utilize option 3, with option 2 as a backup.

Our requirement of a small ($\approx$ 2 mm rms) spot size for the proton beam as it intercepts the mercury jet favors option 3 over option 2. Site 3 is somewhat more remote from access to the surface, an advantage in terms of radiation safety, but the DC power and cryogenic transfer lines are thereby somewhat more costly. It may be desirable to drill one or more penetrations in the walls between the TT2A and TT2 tunnels to shorten the length of the cryogenic transfer lines.

The high-speed camera that views the mercury jet must be shielded from radiation, and cannot readily be located in the TT2A tunnel. However, it should be possible to place the camera in the TT2 tunnel, behind existing concrete shielding, as indicated in Fig. 34.

Figures 38 and 39 show additional details of possible arrangements of the DC power lines and cryogenic transfer lines.

2.2.1 nTOF Beamline Issues

Although the proposed experiment is to operate in a pulse-on-demand mode with only 100-200 proton pulses over a two-week period, we do not propose to run parasitically to the nTOF program. Rather, the proposed experiment should have a dedicated running period.

A strong motivation for dedicated running concerns possible activation of the titanium Ti-6Al-4V alloy proton-beam windows of the mercury containment vessel. While activation of these windows is a minor issue during the small number of pulses of this experiment, these windows would incur considerable activation if they were in the beam during regular nTOF

Figure 35: Photographs of option 1 for siting of the proposed target test facility.

Figure 36: Photographs of options 2 and 3 for siting of the proposed target test facility.

running.

We desire the highest proton momentum compatible with programmable fast extraction from the PS, and transport down the nTOF line. While the nTOF program typically runs with a 20 GeV/c proton beam, we prefer to use a 24 GeV/c beam, which also argues for a dedicated run of this experiment.

Furthermore, our request for a small proton beam spot will be easier to achieve without the longitudinal bunch compression normally used during nTOF running (to decrease the width of the neutron time-of-flight distribution).

We are requesting up to 2×10^{13} protons in a single fast-extracted spill. This intensity, combined with the increase in energy from 20 to 24 GeV, may exceed the capacity of the present nTOF target station, which would be functioning as the beam dump for our experiment. Therefore it may be desirable to add a temporary increase in shielding of the nTOF target/dump during the running of our experiment.

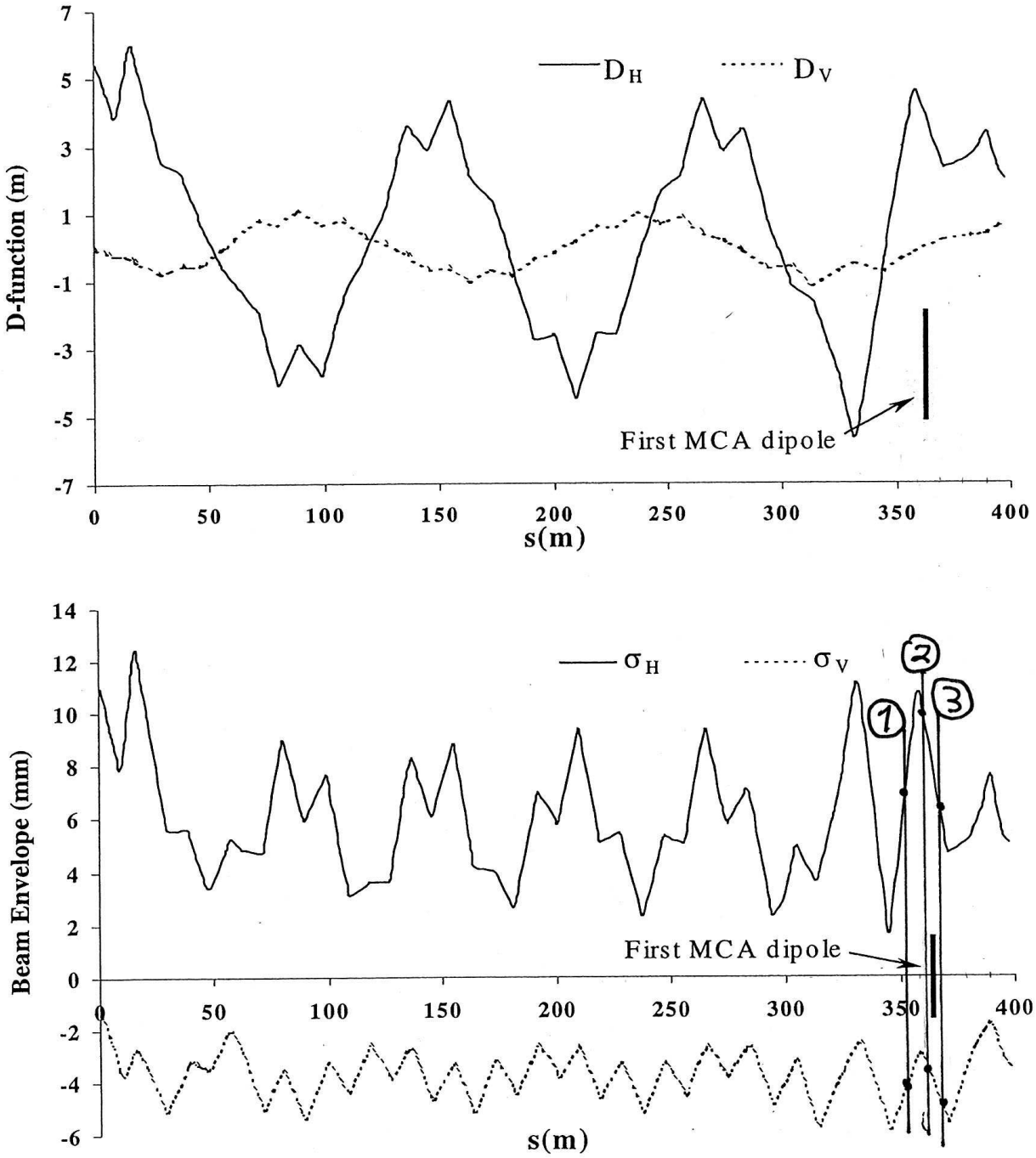

Figure 37: Dispersion and spot size *vs.* position along the nTOF beamline [60]. The three candidate locations are at 352, 363, and 372 m, where intermediate foci are located. We proposed to run the proton beam without the longitudinal bunch compression presently used by the nTOF program, which should reduce the horizontal dispersion, and the horizontal spot sizes, by about a factor of two.

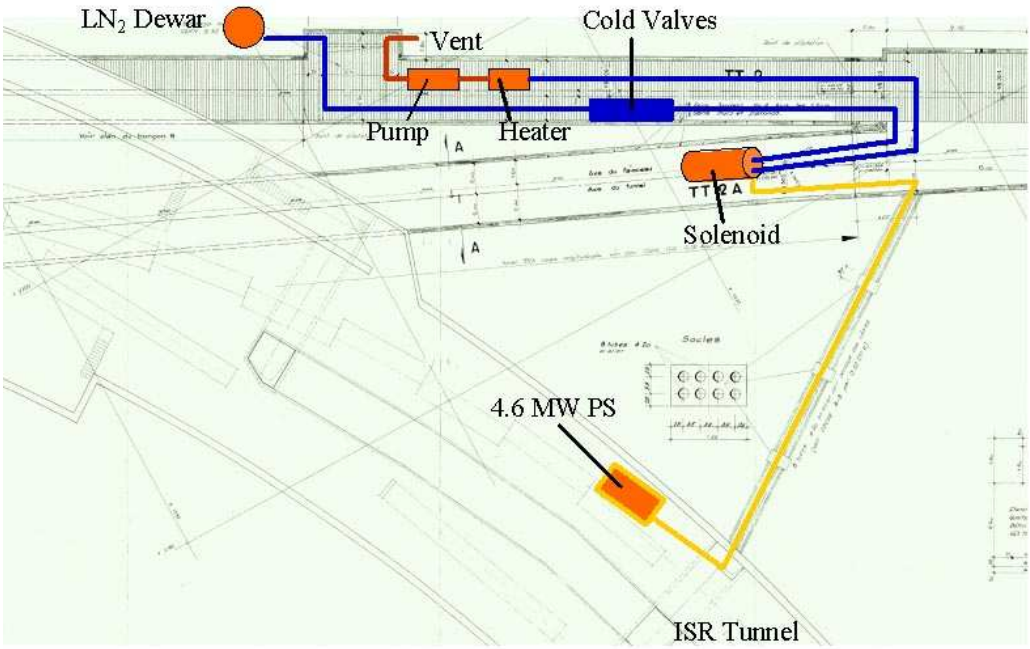

Figure 38: Plan view of a possible arrangement of DC power lines and the cryogenic transfers, with the solenoid magnet at the location of option 2. The 4.6 MW power converter could reside in the ISR tunnel, with the DC bussing passing through an existing 2-m high horizontal access shaft to the TT2A tunnel. The cryogenic transfer lines would pass along the TT2 tunnel and up the vertical access shaft to 6,000 l dewar on the surface.

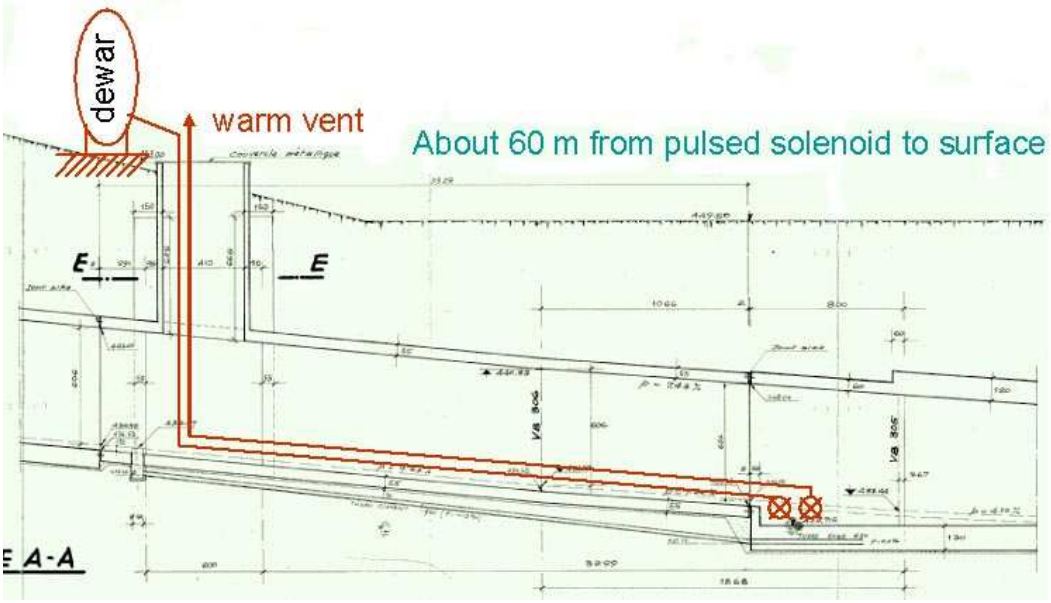

Figure 39: Elevation view of the sloping TT2 tunnel and the associated vertical access shaft. The cryogenic transfer lines are shown for option 1.

As indicated in Fig. 21, the proton beam crosses the mercury jet at an angle of 33 mrad so that the proton beam will not hit the nozzle of the jet, which is located 50 cm upstream of the center of the interaction region. Furthermore, the yield of soft pions from the proton-mercury interaction is enhanced if the beam and jet are tilted with respect to the axis of the solenoid magnet, as shown in Fig. 3d. Hence, the proof-of-principle test of the mercury jet plus solenoid should include such a tilt of the proton beam axis.

If we tilt the magnetic axis by 67 mrad with respect to the proton beam in the horizontal plane, as indicated in Fig. 21, then the proton beam will experience a horizontal field integral of 1 T-m as is passes through the 1-m-long 15-T solenoid. As a result the beam will experience a 300 MeV/c vertical kick, which is 12.5 mrad for a 24 GeV/c beam.

Should the experiment at the location of option 3, some 20 m upstream of the nTOF target station, the proton beam would be deflected vertically by 25 cm there. To avoid this large displacement, a vertical trim magnet with 1 T-m field integral should be installed just downstream of the 15-T solenoid to compensate for the vertical kick of the latter. Should this not be possible, we will consider operation of the experiment with the proton beam coincident with the magnetic axis, although that is not our preference.

Of course, the 15-T solenoid acts on the proton beam like a (weak) lens even when the beam axis coincides with the magnetic axis. The Larmor wavelength for 24 GeV/c protons is $\lambda\!\!\!^{-} = cP/eB = 5.33$ m, so the focal length of the 1-m-long solenoid is $f = 4\lambda\!\!\!^{-2}/L = 114$ m. Since the focal length is longer than the distance from the solenoid to the nTOF target/dump, the solenoid focusing will have negligible effect on the proton beam transport.

2.2.2 Run Plan

We propose to occupy the 3m clear space in the TT2A tunnel of the nTOF proton transfer line some 20 m downstream of the entrance into the TT2A tunnel area (Option 3). Siting option 2 remains under consideration as a backup.

We propose to set up the experiment during the 2005 shutdown of the PS, run the experiment in a dedicated mode for the initial two weeks of PS operations in 2006 (likely to be April 2006), and then remove those components in the experiment which could possibly obstruct the proton beam in its path to the nTOF target. These items will include the beam-profile monitors, the stainless-steel double-containment vessel and its proton-beam windows, the optical mirrors within the containment vessel, and of course the mercury and the mercury recirculation system. Also to be removed will be a temporary beam stop which will be inserted to protect the nTOF target station from possible damage due to the high intensity of the proton beam.

The mercury will be provided by Oak Ridge National Laboratory, which will also take responsibility for its disposal on completion of the experiment.

Our run plan calls for a total of 38 spills in which the mercury jet interacts with the proton beam from the PS, with beam intensities from 5 TP (5×10^{12} protons) to 20 TP. Details are presented in Table 2. Since an individual rf bucket of the PS can accelerate a maximum of 5 TP, the PS will need to operate with 1-4 rf buckets to meet our requirements. Applying a 50 % contingency, there will be a maximum of 60 spills with proton-mercury interactions. We estimate that the total protons-on-target will be 800×10^{12}, which is the number used in the calculation of materials activation presented in the following section.

Table 2: Requested Proton Pulses for Interaction with the Mercury Jet. The rf bucket structure of the PS is varied to simulate the effect of higher proton intensities than can be delivered in a single rf bucket, and to explore the effect of very long proton pulses.

Number of Protons	rf Bucket Structure	Solenoid Field (T)	Horizontal Beam Offset (mm)	Number of Spills
4×5 TP	1-2-3-4	0	0	2
4×5 TP	1-2-3-4	5	0	2
4×5 TP	1-2-3-4	10	0	2
4×5 TP	1-2-3-4	15	0	2
4×5 TP	1-2-3-4	15	+5	2
4×5 TP	1-2-3-4	15	+2.5	2
4×5 TP	1-2-3-4	15	−2.5	2
4×5 TP	1-2-3-4	15	−5	2
1×5 TP	1	15	0	2
2×5 TP	1-2	15	0	2
3×5 TP	1-2-3	15	0	2
4×5 TP	1-2-3-5	0	0	2
4×5 TP	1-2-3-5	15	0	2
4×5 TP	1-2-3-6	0	0	2
4×5 TP	1-2-3-6	15	0	2
4×5 TP	1-2-3-7	0	0	2
4×5 TP	1-2-3-7	15	0	2
4×5 TP	1-2-3-8	0	0	2
4×5 TP	1-2-3-8	15	0	2
Total				38

The run plan presented in Table 2 includes a set of 8 spills in which the beam is scanned horizontally across the mercury jet. For this the magnet will need to be mounted on a movable stage.

This program will explore the effects of target disruption as a function of both beam intensity and magnetic field strength, issues that are critical for the design of future high-power targets.

We will also explore temporal aspects of high-intensity beam/target interactions by varying the bucket structure of the PS spill. This pump-probe capability of the PS beam is unique in the world at this time. As indicated in Table 2, the set of spills with a variable time interval between the third and fourth extracted rf bucket will include both magnet-on and magnet-off pulses. The latter are relevant to the use of a mercury target with a neutrino horn, as foreseen in a neutrino factory based on a proton linac [3].

In addition to the $\approx$ 60 spills in which the mercury jet will interact with the proton beam, we will require of order 100 proton spills for beam tuning, during which the mercury jet would be turned off. The solenoid magnet will be pulsed during a few of these tuning spills to verify the effect of the solenoid field on the proton beam.

The cooling cylce of our pulsed solenoid will allow for a magnet-on proton interaction every 30 minutes. Hence, we can comfortably conclude the experiment within a two week period.

2.2.3 Activation Issues

Activation of material in and about the solenoid magnet by the proton beam has been simulated in a MARS calculation that include the effect of the 15-T magnetic field [23, 62]. Assuming 40 interactions of 24-GeV protons with the mercury jet, each with 20 TP intensity, there are a total of 8×10^{14} protons incident during a 14 day period. The resulting contact radiation level at a magnetic element 1 m downstream of the solenoid magnet is given in Table 3. The calculated contributions to the radiation levels by various spallation products in the mercury target are given in Table 4.

Table 3: Calculated radiation level at a magnetic element 1 m downstream of the 15-T solenoid, after 8×10^{14} 24-GeV protons incident on the mercury jet target over a 14-day period. From [62].

Time	Contact Radiation Level
After 1 hr	10 mrad/hr
After 1 day	5 mrad/hr
After 1 week	3 mrad/hr
After 1 mo.	1 mrad/hr
After 1 year	250 μrad/hr

Table 4: Contributions of various elements produced in the mercury target to the calculated radiation level, 1 month and 1 year after the end of the run.

Element	Curies after 1 mo.	Curies after 1 year
Hg	11×10^{-5}	$< 2.4 \times 10^{-6}$
Au	8.5×10^{-5}	2.9×10^{-5}
Te	7.0×10^{-5}	$< 2.4 \times 10^{-6}$
Ir	6.9×10^{-5}	$< 2.4 \times 10^{-6}$
Cd	$< 3.0 \times 10^{-5}$	1.2×10^{-5}
Ag	6.7×10^{-5}	1.2×10^{-5}
In	5.9×10^{-5}	1.2×10^{-5}
Sn	5.9×10^{-5}	1.2×10^{-5}
Eu	4.5×10^{-5}	$< 2.4 \times 10^{-6}$
Rh	4.5×10^{-5}	$< 2.4 \times 10^{-6}$
I	3.7×10^{-5}	$< 2.4 \times 10^{-6}$
Xe	3.5×10^{-5}	$< 2.4 \times 10^{-6}$
Ta	$< 3.0 \times 10^{-5}$	4.8×10^{-6}
Gd	3.1×10^{-5}	4.2×10^{-6}
Pd	3.1×10^{-5}	$< 2.4 \times 10^{-6}$
Cs	3.0×10^{-5}	$< 2.4 \times 10^{-6}$
Lu	$< 3.0 \times 10^{-5}$	3.4×10^{-6}
Os	$< 3.0 \times 10^{-5}$	3.2×10^{-6}
Ce	$< 3.0 \times 10^{-5}$	3.1×10^{-6}
Rh	$< 3.0 \times 10^{-5}$	2.9×10^{-6}
Pm	$< 3.0 \times 10^{-5}$	2.7×10^{-6}
W	3.0×10^{-5}	2.7×10^{-6}
Sm	$< 3.0 \times 10^{-5}$	2.6×10^{-6}
Hf	$< 3.0 \times 10^{-5}$	2.4×10^{-6}
Total	1.1×10^{-3}	1.2×10^{-4}

2.3 Budget and Schedule

A schedule for the proposed experiment is shown in Fig. 40, featuring installation in the TT2A tunnel in the fourth quarter of 2005, with commissioning in the first quarter of 2006, followed by a 2-week run in April 2006. A preliminary estimate of the manpower effort and required funding for the experiment is shown in Table 5

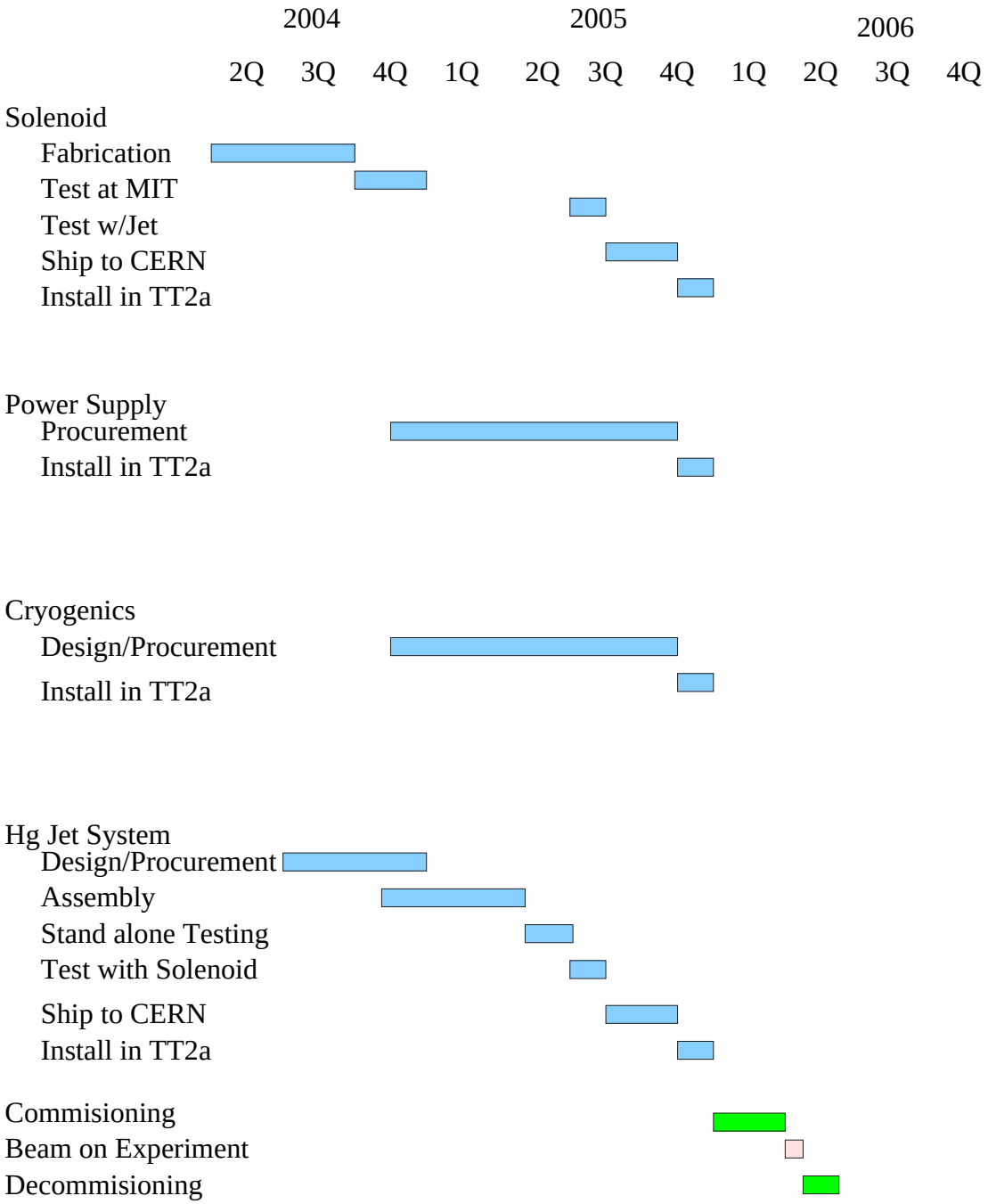

Figure 40: Projected schedule for the proposed experiment.

Table 5: Projected effort and cost for the proposed experiment.

		Cost US k$	Effort Man*Mo
Solenoid			
	Testing	90	2
	Shipping	15	1
	Installation	20	1
	Decommisioning	25	1
Power Supply			
	Engineering Support	50	3
	Procurement	300	2
	Installation	80	1
	Decommisioning	20	1
	Contingency	70	
Cryogenics			
	Engineering Support	45	4
	Procurements	50	1
	Controls	40	2
	Installation	110	6
	Decommisioning	10	1
	Contingency	40	
Hg Jet			
	Engineering Support	30	12
	Components	30	6
	Optical System	35	12
	Windows	15	2
	Decomminsioning	20	1
	Contingency	20	
Beam Systems			
	Profile/Position	40	3
	Dump	25	3
	Scintillators	10	2
Support Services			
	Data Acquistion	40	3
	Proj. Management	150	24
Total		1380	94

3 References

[1] A. Blondel *et al.*, *Superbeam Studies at CERN*, CERN-NUFACT-Note-95 (Oct. 8, 2001), slap.web.cern.ch/slap/NuFact/NuFact/nf95.pdf

[2] Y. Hayato *et al.*, *Neutrino Oscillation Experiment at JHF*, Letter of Intent 12 to the J-PARC 50 GeV Proton Synchrotron (Jan. 21, 2003), psux1.kek.jp/ jhf-np/LOIlist/pdf/L12.pdf

[3] P. Gruber *et al.*, *The Study of a European Neutrino Factory Complex*, CERN/PS/2002-080 (PP) (Dec. 2002), slap.web.cern.ch/slap/NuFact/NuFact/nf122.pdf

[4] M.M. Alsharo'a *et al.*, *Status of Neutrino Factory and Muon Collider Research and Development and Future Plans*, Phys. Rev. ST Accel. Beams **6**, 081001 (2003).

[5] S. Machida *et al.*, *The Prism Project*, Letter of Intent 24 to the J-PARC 50 GeV Proton Synchrotron (Jan. 1, 2003), psux1.kek.jp/~jhf-np/LOIlist/pdf/L24.pdf

[6] The MECO experiment home page: http://meco.ps.uci.edu/

[7] S. Machida *et al.*, *PRIME: An Experimental Search for the* $\mu^- \to e^-$ *Conversion Process at an Ultimate Sensitivity of the Order of* 10^{-18} *with PRISM*, Letter of Intent 25 to the J-PARC 50 GeV Proton Synchrotron (Jan. 1, 2003), psux1.kek.jp/~jhf-np/LOIlist/pdf/L25.pdf

[8] A. Silenko *et al.*, *Search for a Permanent Muon Electric Dipole Moment at the* 10^{-24} *e-cm Level*, Letter of Intent 22 to the J-PARC 50 GeV Proton Synchrotron (Jan. 9, 2003), psux.kek.jp/~jhf-np/LOIlist/pdf/L22.pdf

[9] Spallation Neutron Source project homepage: www.sns.gov/projectinfo/projectinfo.htm

[10] The European Spallation Source documentation page: www.neutron-eu.net/en/index.php?cat=93&id=110

[11] J-PARC Materials and Life Science Facility home pages: http://j-parc.jp/MatLife/en/index.html www.jaeri.go.jp/english/research/re06.html

[12] Advanced Fuel Cycle home page: apt.lanl.gov/index.html

[13] Accelerator Transmutation of Waste Roadmap: www.pnl.gov/atw/

[14] R. Ferdinand, *IFMIF – A challenging high intensity accelerator* (Apr. 8, 2002), http://www.hep.princeton.edu/~mcdonald/mumu/target/tue_wg2_ferdinand_IFMIF.pdf JAERI-IFMIF home page: insdell.tokai.jaeri.go.jp/IFMIFHOME/ifmif_home_e.html

[15] J. Lettry *et al.*, *Experience with ISOLDE Molten Metal Targets at the CERN-PS Booster*, in Proceedings of ICANS-XIII (1995), www.hep.princeton.edu/~mcdonald/mumu/target/lettry/1.html

[16] J.R. Haines, *Pitting Issues/Target Decision*, (Nov. 13, 2002), www.hep.princeton.edu/~mcdonald/mumu/target/ORNL/Haines_DOE_Nov_02.pdf

[17] *Status Report on Mercury Target Development and Related Issues*, SNS-101060100-TR0006-R00 (July 31, 2002), www.hep.princeton.edu/~mcdonald/mumu/target/ORNL/pitting.pdf

[18] C.D. Johnson, *Present and Future Possibilities of Antiproton Production from Fixed Targets at CERN*, Hyperfine Interactions **44**, 21 (1988).

[19] R.M. Dzhikibaev and V.M. Lobashev, *On the search for the $\mu \to e$ conversion process in a nucleus*, Sov. J. Nucl. Phys. **49**, 384 (1989).

[20] R.B. Palmer *et al.*, *Muon Colliders*, A.I.P. Conf. Proc. **372**, 3 (1996).

[21] S. Ozaki *et al.*, eds., *Feasibility Study-II of a Muon-Based Neutrino Source*, Chap. 3 discusses the target system. (June 13, 2001), www.cap.bnl.gov/mumu/studyii/FS2-report.html

[22] N.V. Mokhov and A. Van Ginneken, *Pion Production and Targetry at $\mu^+\mu^-$ Colliders*, AIP Conf. Proc. **441**, 320 (1998); www-ap.fnal.gov/~mokhov/papers/1998/Fermilab-Conf-98-41.ps
N.V. Mokhov and S.I. Striganov, *Model for Pion Production in Proton-Nucleus Interactions*, FERMILAB-Conf-98/053 (Feb. 5, 1998); www-lib.fnal.gov/archive/1998/conf/Conf-98-053.html

[23] N.V. Mokhov, *The MARS Code System Usersí Guide*, Fermilab-FN-628 (1995), www-ap.fnal.gov/MARS/

[24] N.V. Mokhov, *Particle Production for a Muon Storage Ring: I. Targetry and π/μ Yield*, Muon Collaboration Note MUC0169 (Sep. 2000), www-mucool.fnal.gov/mcnotes/muc0169.pdf

[25] P.T. Spampinato *et al.*, *Support Facility for a Mercury-Jet Target Neutrino Factory*, ORNL/TM-2001/124 (Sept. 2001), www.hep.princeton.edu/~mcdonald/mumu/target/tm-2001-124.pdf

[26] P. Sievers and P. Pugnat, *Response of Solid and Liquid Targets to High Power Proton Beams for Neutrino Factories*, CERN-NuFACT Note 035 (Oct. 12, 2000), nicewww.cern.ch/~molat/neutrino/nf35.pdf

[27] J. Gallardo *et al.*, *First order perturbative calculations for a conducting liquid jet in a solenoid*, MUC0242 (Apr. 12, 2002), www-mucool.fnal.gov/mcnotes/public/pdf/muc0242/muc0242.pdf

[28] J.R. Haines *et al.*, *Summary of Mercury Target Pitting Issue*, SNS-101060100-TR0004-R00 (April, 2002), sec 4.0. This document forms Appendix of [17].

[29] R. Samulyak, *Numerical simulation of hydro- and magnetohydrodynamic processes in the Muon Collider target*, Lecture Notes in Comp. Sci. **2331** (Springer-Verlag, Berlin, 2002), pp. 391-400.

[30] R. Samulyak *et al.*, *Numerical Simulation of Free Surface MHD Flows: Richtmyer - Meshkov Instability and Applications*, Lecture Notes in Comp. Sci. **2667** (Springer-Verlag, Berlin, 2003), pp. 558-567.

[31] R. Samulyak, Y. Prykarpatskyy, *Richtmyer-Meshkov instability in liquid metal flows: influence of cavitation and magnetic fields*, Mathematics and Computers in Simulations (2004), www.sciencedirect.com/science/article/B6V0T-4BWYT41-1/2/c8e054b4e348d716223e75bcad9ca378)

[32] FronTier code home page: www.ams.sunysb.edu/~shock/FTdoc/FTmain.html

[33] Lord Rayleigh, *The Theory of Sound* (reprinted by Dover, 1945), Vol. 2, p. 362.

[34] S. Chandrasekhar, *Hydrodynamic and Hydromagnetic Stability* (reprinted by Dover, 1981), §112.

[35] J. Alessi *et al.*, *An R&D Program for Targetry and Capture at a Muon-Collider Source* (Sep. 29, 1998, approved as BNL E-951 Oct. 1, 1999), www.hep.princeton.edu/~mcdonald/mumu/target/targetprop.pdf

[36] CERN/ISOLDE Mass Separator Facility home page: isolde.web.cern.ch/ISOLDE/

[37] Grenoble High Field Magnet Laboratory home page: ghmfl.polycnrs-gre.fr/

[38] FISO Technologies home page: www.fiso.com/

[39] N. Simos *et al.*, *Thermal Shock Induced by a 24 GeV Proton Beam in the Test Windows of the Muon Collider Experiment E95 – Test Results and Theoretical Predictions*, contributed to AccAPP'01 (Nov. 9, 2001), www.hep.princeton.edu/~mcdonald/mumu/target/simos/e951_windows_AccAPP2001.pdf

[40] N. Simos *et al.*, *E951 Experiment Target Response Re-Evaluation* (May 10, 2002), www.hep.princeton.edu/~mcdonald/mumu/target/simos/NSimos_Shelter_presentation.pdf

[41] N. Simos *et al.*, *Study of Graphite Targets Interacting with the 24 Gev Proton Beam of the BNL Muon Target Experiment*, contributed to EPAC2002 (May 24, 2002), www.hep.princeton.edu/~mcdonald/mumu/target/simos/TUPDO024.pdf

[42] P. Thieberger, *Upper Limits for Sublimation Losses from Hot Carbon Targets in Vacuum and in Gases*, MUC0186 (Nov. 27, 2000), www-mucool.fnal.gov/mcnotes/public/pdf/muc0186/muc0186.pdf

[43] J.R. Haines and C.C. Tsai, *Graphite Sublimation Tests for the Muon Collider/Neutrino Factory Target Development Program* (Nov. 7, 2001), www.hep.princeton.edu/~mcdonald/mumu/target/Graphite_Sublimation_Report.pdf

[44] T. Saito *et al.*, *Multifunctional Alloys Obtained via a Dislocation-Free Plastic Deformation Mechanism*, Science **300**, 464 (2003).

[45] H.G. Kirk *et al.*, *Super-Invar as a Target for a Pulsed High-Intensity Proton Beam*, presented at PAC2003 (May 12, 2003), warrior.lbl.gov:7778/pacfiles/papers/TUESDAY/PM_POSTER/TPPB002/TPPB002.PDF

[46] H.G. Kirk, *Summary of the Workshop on High-Power Targetry for Future Accelerators* (Ronkonkoma, NY, Sept. 8-12, 2003), pubweb.bnl.gov/people/kirk/e951/cern_nov_03/cern_targetry.pdf Workshop presentations: www.cap.bnl.gov/mumu/conf/target-030908/agenda.xhtml

[47] N. Simos *et al.*, *Material Studies of Pulsed High-Intensity Proton Beam Targets*, presented at ICONE12 (Arlington, VA, Apr 26, 2004), www.hep.princeton.edu/~mcdonald/mumu/target/simos/ICONE12_49441.pdf

[48] A. Hassanein *et al.*, *An R&D program for targetry and capture at a neutrino factory and muon collider source*, Nucl. Instr. and Meth. **A503**, 70 (2003).

[49] K.T. McDonald *et al.*, *The R&D Program for Targetry at a Neutrino Factory*, paper TPAH156 contributed to PAC2001 (Jun 18, 2001), www.hep.princeton.edu/~mcdonald/mumu/pac01/tpah156.pdf

[50] H.G. Kirk *et al.*, *Target Studies with BNL E951 at the AGS*, paper TPAH137 contributed to PAC2001 (Jun 18, 2001), www.hep.princeton.edu/ mcdonald/mumu/pac01/tpah137.pdf

[51] A. Fabich, *High Power Proton Beam Shocks and Magnetohydrodynamics in a Mercury Jet Target for a Neutrino Factory*, Ph.D. Thesis, Technischen Universität Wien (Nov. 2002), www.hep.princeton.edu/~mcdonald/mumu/target/thesis-2002-038.pdf

[52] N. Simos *et al.*, *Interaction of a 24-GeV Proton Beam with a Muon-Collider Mercury Jet Target. Experimental Results and Thermodynamic Assessment*, submitted to AccApp'01 (Nov. 9, 2001), www.hep.princeton.edu/~mcdonald/mumu/target/simos/e951_jet_AccAPP2001.pdf

[53] R.J. Weggel, *A Three Stage Cryogenic Pulse Magnet Program for the BNL Targetry Experiment* (Feb. 9, 2002), www.hep.princeton.edu/~mcdonald/mumu/target/weggel/chicago_020902.pdf

[54] P. Titus, *E-951 15-T Pulsed Magnet for Mercury Target Development* (Sept. 6, 2002), www.hep.princeton.edu/~mcdonald/mumu/target/MIT/desrev_090602.pdf

[55] P. Titus' web page "BNL Pulsed Magnet Memos and Reports", www.psfc.mit.edu/people/titus/#BNL Memos

[56] P. Titus, *Pulsed Magnet Status* (Apr 13, 2004), www.hep.princeton.edu/~mcdonald/mumu/target/MIT/titus_041304.pdf

[57] P. Titus, *E-951 15-T Pulsed Magnet Cooldown Times* (Jan. 22, 2003), www.hep.princeton.edu/~mcdonald/mumu/target/MIT/Hegas.pdf

[58] C.A. Martins, *Analysis of the Possibility of Using an Alice/LHCb Type Power Converter in TT2A Target Test* (Mar 31, 2004), http://www.hep.princeton.edu/~mcdonald/mumu/target/CERN/Meeting_nTOF_31032004.pdf The LHC spec for the power converter is EDMS 311284, the spec for the transformer is EDMS 315101.

[59] J.R.J. Bennett *et al.*, *Studies of a Target System for a 4-MW, 24-GeV Proton Beam*, Letter of Intent to the CERN INTC (Oct. 23, 2003), http://www.hep.princeton.edu/~mcdonald/mumu/target/cern_loi.pdf

[60] M. Giovannozzi, *Alternative Layout of the Transfer Line for the Time-of-Flight Neutron Facility at the CERN-PS*, PS/CA/Note99-17 (22 July 1999).

[61] S. Adrianmonje *et al.*, *Neutron TOF Technical Design Report*, CERN/INTC/2000-004 (11 February 2000), cdsweb.cern.ch/search.py?recid=429174

[62] H.G. Kirk, *Summary of Dose Calculations for the CERN High-Power Target Experiment* (April 23, 2004), http://pubweb.bnl.gov/people/kirk/e951/cern_proposal/dose_update.ppt